UNIVERSIDAD DE CHILE
FACULTAD DE CIENCIAS FÍSICAS Y MATEMÁTICAS
DEPARTAMENTO DE INGENIERÍA MECÁNICA

MULTI-LEVEL BAYESIAN ANALYSIS OF PIEZOELECTRIC ENERGY HARVESTERS

TESIS PARA OPTAR AL GRADO DE
MAGÍSTER EN CIENCIAS DE LA INGENIERÍA, MENCIÓN MECÁNICA

ALEJANDRO JOSÉ POBLETE ANDRADES

PROFESOR GUÍA:
DR. RAFAEL RUIZ GARCÍA

MIEMBROS DE LA COMISIÓN:
DR. GAOFENG JIA
DR. VIVIANA MERUANE NARANJO

Este trabajo ha sido financiado por
ANID Becas/Magíster Nacional 22211050

SANTIAGO DE CHILE
2022

RESUMEN DE LA TESIS PARA OPTAR
AL GRADO DE MAGÍSTER EN CIENCIAS
DE LA INGENIERÍA, MENCIÓN MECÁNICA
POR: ALEJANDRO JOSÉ POBLETE ANDRADES
FECHA: 2022
PROF. GUÍA: DR. RAFAEL RUIZ GARCÍA

ANÁLISIS BAYESIANO MULTINIVEL DE RECOLECTORES DE ENERGÍA PIEZOELÉCTRICOS

Este trabajo propone un esquema bayesiano jerárquico para identificar propiedades electromecánicas en recolectores de energía piezoeléctricos (PEHs, por su sigla en inglés) e incertidumbres asociadas basadas en funciones respuesta en frecuencia (FRFs) experimentales. El esquema permite el uso de datos experimentales de múltiples dispositivos, potencialmente definidos por diferentes propiedades electromecánicas. En el esquema jerárquico propuesto, la dispersión de la FRF observada en grupos de PEHs es explícitamente modelada como consecuencia de las incertidumbres en los parámetros del modelo, más que como una consecuencia únicamente del error de predicción del modelo, algo típicamente obtenido en el esquema bayesiano clásico. El método Transitional Markov Chain Monte Carlo (TMCMC) se utiliza para identificar la distribución posterior de los parámetros del modelo. La preferencia hacia el esquema jerárquico es luego confirmada utilizando el procedimiento de selección de modelos bayesiano (Bayesian model class selection), para comparar las probabilidades posteriores de seleccionar el esquema jerárquico o clásico. El marco propuesto es aplicado para la identificación de parámetros tanto en un solo dispositivo como en grupos de dispositivos. Los resultados muestran que el esquema jerárquico propuesto presenta ventajas significativas en comparación con otros enfoques bayesianos aplicados a PEHs. Primero, permite el uso de datos experimentales de multiples dispositivos para actualización de parámetros; segundo, considera correctamente las incertidumbres de los parámetros a través de múltiples dispositivos; tercero, podría usarse para identificar densidades de probabilidad previas objetivas en un enfoque bayesiano clásico.

RESUMEN DE LA TESIS PARA OPTAR
AL GRADO DE MAGÍSTER EN CIENCIAS
DE LA INGENIERÍA, MENCIÓN MECÁNICA
POR: ALEJANDRO JOSÉ POBLETE ANDRADES
FECHA: 2022
PROF. GUÍA: DR. RAFAEL RUIZ GARCÍA

MULTI-LEVEL BAYESIAN ANALYSIS OF PIEZOELECTRIC ENERGY HARVESTERS

This work proposes a hierarchical Bayesian framework to identify electromechanical properties of Piezoelectric Energy Harvesters (PEHs) and associated uncertainties based on experimental frequency response functions (FRFs). The framework allows the use of experimental data from multiple devices, potentially defined by different electromechanical properties. In the proposed hierarchical scheme, the FRF dispersion experimentally observed in groups of PEHs is explicitly modeled as a consequence of uncertainties in the model parameters rather than as a consequence of only the model prediction error typically used in classical Bayesian scheme. The Transitional Markov Chain Monte Carlo (TMCMC) method is used to establish the full posterior distribution of the model parameters. Preference towards selection of the hierarchical scheme is further confirmed by using Bayesian model class selection to compare the posterior probabilities of selecting the hierarchical or the classical scheme. The proposed framework is applied to identification of model parameters for both a single device and groups of devices. Results show that the proposed hierarchical scheme present significant advantages compared to other Bayesian based approaches for PEHs. First, it allows the use of experimental data from multiple devices for model parameter updating; second, it accounts for the model parameter uncertainties across different devices; third, it could be used to identify objective priors for a classical Bayesian approach.

a Cachito

Acknowledgments

Primero, quisiera agradecer a mi familia, a mi papá, mamá, hermano que extraño mucho y cachito. También agradecer a mi polola Li Quen que siempre me apoyó durante este proceso. Los amo.

Un reconocimiento especial para mis amigos de plan común, que desde 2014 nos vimos envueltos en un sinfin de situaciones: Ángela, Feña (ahora novios), Claudio, Fabi, PL, Ignacio Antonio Pino, Sergio, Tania, Carlos, Cristian, Max, Vicente, Franco, Jorge, Santiago, Hans. Vaya un gran saludo cordial para ellos.

También recordar a mis entrañables amigos del DIMEC, Ignacio, Diego H., Daniel, Pancho, Pablo, Pau, Yon, Cristian, Chino, Franco, Nico, Doña, Bruno.

A mis amigos del colegio, con quienes a pesar de los años, nos seguimos viendo como siempre. Un salud. Mención especial para los grandes amigos de la vida Benjamín *men* y Simón.

A la comisión de Magíster de este trabajo, partiendo por el profesor guía Rafael Ruiz, que me enseñó este mundo de incertidumbres en ingeniería y confió en mis habilidades para llevar a cabo este proyecto. Gracias por todas las oportunidades brindadas, de seguro seguiremos trabajando juntos. Also, I would like to thank Dr. Gaofeng Jia for accepting being part of this work and for his insightful comments. También agradecer a la profesora Viviana Meruane por ser parte de la comisión evaluadora y su apoyo en este proceso.

Finalmente, también agradecer a ANID por el apoyo económico a este trabajo bajo la beca ANID BECAS/MAGISTER NACIONAL 22211050.

Table of Content

List of Tables

List of Figures

Chapter 1

Introduction

In the last two decades, the use of piezoelectric materials for energy harvesting applications has raised the attention of the scientific community [1]. Different devices have been proposed to facilitate the energy scavenging in vibratory environments, with the cantilever piezoelectric beam type being the most common piezoelectric energy harvester (PEH) configuration. In these devices, the cantilever beam is composed of a main elastic layer (wide range of non piezoelectric materials have been used) bonded to another layer of piezoelectric material. The energy harvesting is accomplished by locating the devices in vibratory environments that induce an oscillatory deformation in the beam [2, 3]. In this way, the strain in the piezoelectric material generates an electric charge while the main elastic layer provides structural support. Depending on the number of piezoelectric layers, the devices are classified as unimorph (one layer) or bimorph (when two layers are bonded to the main elastic layer) [4]. A general scheme of the latter configuration is shown in Figure 1.1.

Multiple and diverse models have been developed to describe and predict the PEHs' electromechanical behavior, including single degree of freedom models [5], electromechanical finite element models [6], reduced-order models (ROMs) [7], isogeometric analyses [8], and linear and nonlinear distributed parameter models [9, 10, 11]. Among the latter, the linear model proposed by Erturk and Inman [10], based on the Euler-Bernoulli beam theory, has became quite popular since it provides clean analytical expressions for the behavior of PEHs by considering the electromechanical coupling.

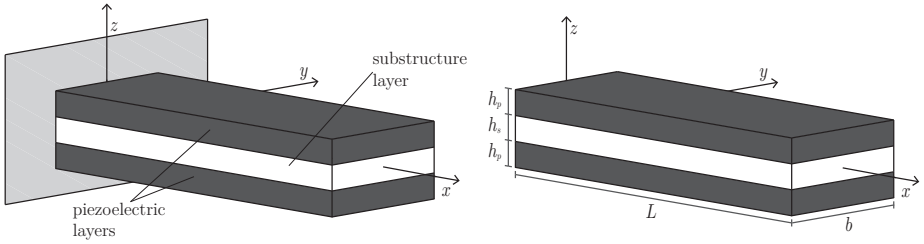

Figure 1.1: Typical scheme of a rectangular Bimorph PEH in a cantilevered condition. Substructure and piezoelectric layers are also shown together with the main geometrical parameters.

Despite the development of high fidelity models, mismatches between numerical and experimental observations are detected when nominal electromechanical properties are used, indicating the need to tune the electromechanical properties of each device based on experimental observations. This conclusion was made by Peralta et al. [12] after studying the dynamic response of a group of PEHs with identical nominal electromechanical properties, raising the concern about the characterization of the uncertainties involved in the electromechanical properties. The study revealed that the most important source of uncertainty is related to the electromechanical properties but no attempt was made to characterize it. However, the authors stated that if these uncertainties are modeled adopting a probability perspective, then, the uncertainties can be propagated to the Frequency Response Function (FRF) by following a procedure previously introduced by Ruiz and Meruane [13]. Given this, the study left open questions about the identification of the electromechanical properties dispersion such that stochastic predictions will be in agreement with the dispersion observed in the FRFs. Particularly, this identification is interesting under two perspectives: (i) in a single PEH to improve its response predictability in future situations and (ii) in multiple same-model PEHs to characterize the uncertainties involved in the material properties. Note that the first task aims to tune the numerical model with respect to experimental observations, which corresponds to an important issue specifically for the validation of new predictive models. On the other hand, the second task aims to improve the precision in the nominal values of the electromechanical properties that is provided by manufacturers as well as their respective variability. Here, the adoption of a Bayesian inference strategy [14] seems to be a natural framework to address these tasks, as it provides the necessary probabilistic context for the electromechanical properties identification.

The Bayesian inference framework, grounded on the probability theory, is a powerful tool to deal with uncertainties in engineering systems modeling. Notably, it provides a framework in which prior information about the model parameters and experimental data are employed to perform a model parameter updating by means of the Bayes theorem. Thus, model parameters are identified as probability density functions (PDFs) conditioned on experimental data (called posterior distribution in the Bayesian context). Ultimately, this process leads to a posterior understanding of the model parameters allowing a robust posterior predictive analysis. Due to the potentially high dimensionality of the model parameters or non linear relationships within the Bayesian formulation, analytical expressions for the posterior distribution are hardly reached. Thus, approximations relying on point estimate values (e.g., applying Laplace asymptotic approximations [15, 16]) or advanced stochastic simulation methods (e.g., Markov Chain Monte Carlo based methods [17, 18]) are usually used. Beyond model parameter updating, the Bayesian inference framework also provides a criterion for selecting the most adequate model among different candidate models, based on experimental data. The procedure, known as model class selection, also enforces a principle of model parsimony, where model accuracy and complexity are balanced (see [19] for more details).

Recently, Peralta et al. [20] explored the implementation of the Bayesian inference framework on a given PEH to fully identify the posterior distribution of the model parameters, addressing the first question proposed in [12]. The results demonstrated the power of the Bayesian method, as it was able to identify the posterior model parameter distribution (electromechanical properties as well as geometrical dimensions) of PEHs to get a mean prediction

that showed an excellent match with the experimental FRFs. The variances of the predicted FRFs were also addressed, observing small variances in all cases studied. Regarding the updated model parameter distribution, large variances were found in their respective marginals. The lower variance at the FRF prediction and high variance at the model parameter marginals was explained by the large correlations found between some model parameters. Similar results were obtained by Poblete et al. [21] when the same framework was applied to PEHs to tune nonlinear constitutive relationships. Overall, it was observed that when applied to a single device Bayesian approach tends to assign large correlation in some model parameters to compensate the large variances found in the marginals. Another important observation made by the authors is the dependency of the updated model parameters on the prior distribution adopted.

The second question proposed in [12] was also addressed recently in [22], in this case, the authors identify that the procedure presented in [20] for updating the model parameters of a single device is not extendable to the case in which the interest is to update the model parameters of a group of multiple same-model PEHs. In this case, the experimental FRF of each PEH studied significantly differs from the other devices of the same group (in particular, presenting different natural frequencies), hence, the FRFs of the group presents a significant dispersion. This motivated the frequency and amplitude normalization of FRFs associated to each device. Then, the authors proposed a multi-output likelihood function (based on the natural frequency, amplitude at natural frequency and normalized FRF) to perform the model parameter updating. Here, the updated model parameters distribution are used to estimate the mean of the FRF as well as its variance. The results show that the predicted mean FRF is in agreement with the observations, however, the predicted FRF variance is considerably lower compared to the experimental evidence. Overall, the procedure presented in [22] allows the identification of model parameters that could be considered representative of the nominal electromechanical properties associated to a group of PEHs. However, the proposed approach was incapable of identifying uncertainties across the devices properly, leaving questions about the actual electromechanical properties variability present in a group of harvesters.

From the Bayesian perspective, it is not surprising that the updated model parameters distribution tends to underestimate the variance of the system output when it is compared to the variance observed experimentally [23, 24]. This is common when multiple experiments are conducted, in particular, when each test slightly differs from the others. Examples of this case could also be found in other structural dynamic problems [25, 26]. According to [26], this is not attributable to the Bayesian methodology itself but an improper formulation of the probabilistic model used to describe the model parameters. In this sense, a new class of probabilistic models had been proposed, referred to as hierarchical Bayesian models [27]. Hierarchical Bayesian models are an extension of the classical Bayesian modeling [28], where an extra level of parameters, called hyperparameters, introduces the hierarchy: they are used to parametrize prior distributions, adding a new information dependency in the model formulation. Depending on information dependence structure, Wu et al. [28] made a distinction between two classes of Bayesian hierarchical models: Hierarchical Prior Model (HPM), which is commonly used to update prior distributions based on experimental data, and Hierarchical Stochastic Model (HSM), where the hyperparameters are used to describe model parameters variations across different data sets. The latter scheme provides a more flexible account for model parameter uncertainties [27] as the different data sets are treated independently.

Recently, hierarchical Bayesian schemes have been adopted in different structural dynamic problems. For example, it has been demonstrated that they are able to account for the inherent variability of structural parameters (e.g., elasticity modulus) due to manufacturing variability [25, 29] and changing environmental/ambient conditions [23, 30]; Sedehi et al. [26] proposed a hierarchical Bayesian model for structural dynamics by breaking up time-series vibration data and adopting novel strategies for posterior identification; Patsialis et al. [31] explored the classical and hierarchical Bayesian schemes to calibrate hysteric reduced order models to agree with high fidelity predictions. Despite the higher complexity and computational cost involved in such a hierarchical Bayesian scheme, its flexibility and potentially better account of uncertainties make its implementation worthwhile [28]. Further, despite the use of hierarchical Bayesian models in structural dynamic problems, its application in the identification of electromechanical properties in PEHs has not been explored, thus, its advantages and disadvantages have not been demonstrated.

Given the above discussions, this work proposes a hierarchical Bayesian approach for the model parameter updating of multiple PEHs. The framework is developed based on the idea of Hierarchical Stochastic Model (HSM), and hyperparameters are used to describe model parameters variations across different devices. The Transitional Markov Chain Monte Carlo (TMCMC) method is used to establish the full posterior distribution of the model parameters. Comprehensive investigations are performed to gain important insights on the performances of the framework. The theoretical implications and details regarding the implementation are presented. Comparison with the classical approach and the impact of informative priors in the model parameter updating are also investigated. The results show an outstanding performance of the proposed hierarchical approach, since: (1) it can capture the uncertainties in model parameters across devices, (2) it can be used to update the model parameters of each device, (3) it offers a probabilistic description of the model parameters that characterize a group of PEHs, and (4) it does not require previous information about the model parameters. In the end, the preference of the hierarchical approach over the classical approach is demonstrated by using Bayesian model class selection.

The rest of the paper is organized as follows. Section 2 reviews piezoelectric energy harvesters, the classical and hierarchical Bayesian schemes' formulations, the model class selection method, and the procedure to achieve robust predictions. Section 3 presents a PEHs' prior parameter uncertainties. Section 4 presents the Bayesian schemes' implementation on multiple and individual PEHs, while Section 5 concludes the study.

Chapter 2

Background

2.1 Piezoelectric energy harvesters (PEHs)

In the last time, efforts have been made to develop alternative methods to get electrical power from ambient energy. The goal is to feed wireless sensors and electronics without requiring electrochemical batteries, which have not experienced a significant development. In this line, the use of piezoelectric materials to harvest energy from vibratory environments has received attention since they present a great power per unit of volume, constituting the so-called piezoelectric energy harvesters.

Energy harvesting by means of piezoelectric materials is achieved due to their oriented molecular structure, which allows a local charge separation (electric dipole). Thus, the application of strain energy to these materials results in an alteration of the dipole, generating an electric charge that can be removed [32]. A typical piezoelectric material used in PEHs is lead zirconium titanate (PZT). On the other hand, the substructure material usually corresponds to a nickel iron alloy, brass, carbon fiber composite, etc.

In order to characterize and quantify the devices' behavior, the Frequency Response Function (FRF) associated to their voltage output is often used. A common forward model that predict this function is reviewed next.

2.1.1 PEH predictive model

In this work, the linear electromechanical model proposed by Erturk and Inman [10] is used. Based on the Euler-Bernoulli beam model, it obtains a simple analytical expression for a PEH response, which is a function of geometric and electromechanical properties of the device:

$$H(\boldsymbol{\theta},\omega) = \left(\frac{i\omega}{i\omega + k_{pzt}}\boldsymbol{\varphi}^{\mathrm{T}}\right)\left[-\mathbf{I}\omega^2 + i\omega\mathbf{C}_{eq} + \mathbf{K}_{eq} + \frac{1}{i\omega + k_{pzt}}\boldsymbol{\chi}\boldsymbol{\varphi}^{\mathrm{T}}\right]^{-1}\mathbf{r} \tag{2.1}$$

The expression is obtained by a modal expansion of N_o eigenvectors of a beam composed of two piezoelectric layers bonded to a central elastic layer, ultimately representing a bimorph

PEH. Then $\mathbf{I}$, $\mathbf{C}_{eq}$ and $\mathbf{K}_{eq} \in \mathbb{R}^{N_o \times N_o}$ correspond to the identity, damping, and stiffness matrices, respectively, and $\boldsymbol{\chi}$, $\boldsymbol{\varphi}$ and $\mathbf{r} \in \mathbb{R}^{N_o}$ are vectors representing electrical coupling, mechanical coupling, and mechanical forcing amplification. The scalar term k_{pzt} incorporates the electrical properties of the harvester. All the mentioned variables (including matrices, vectors, and scalars) are directly dependent on the geometric and mechanical properties of the PEH, which are explicitly shown in Annex A. In this way, the PEHs model predictor is fully defined by the following model parameter vector $\boldsymbol{\theta}$:

$$\boldsymbol{\theta} = \begin{bmatrix} \zeta & s_{11}^E & d_{31} & \varepsilon_{33}^T & \rho_p & \rho_s & E_s & L & b & h_s & h_p \end{bmatrix} \tag{2.2}$$

The model parameters correspond to damping ratio ζ, the elastic compliance at constant electric field s_{11}^E, the piezoelectric constant d_{31}, the permittivity at constant stress ε_{33}^T, the piezoelectric layers density ρ_p, the substructure layer density ρ_s, the elastic modulus of the substructure E_s, the length L, width b, thickness of the substructure layer h_s, and thickness of the piezoelectric layers h_p.

2.2 Bayesian inference

One way to approach uncertainties in engineering models is through the Bayesian Inference framework. Under this framework, experimental data is employed to infer model parameters by using the classical Bayes theorem. Given this probabilistic approach, model parameters are characterized by probability distribution functions (PDF). The method updates the initial knowledge (prior PDF) of the parameters to a posterior understanding, conditioned on experimental data. Besides, Bayesian Inference leads to the selection of the best model class given experimental data, balancing accuracy and complexity of the model.

Next, the classical and hierarchical schemes of the Bayesian inference framework for model parameter updating are presented, as well as the model class selection procedure and the Transitional Markov Chain Monte Carlo (TMCMC) used to establish the posterior PDF.

2.2.1 Classical Bayesian scheme

Consider a predictive model $H(\boldsymbol{\theta}, u) \in \mathbb{R}$ defined by model parameters $\boldsymbol{\theta} \in \mathbb{R}^{N_\theta}$ and input $u \in \mathbb{R}$. Typically, in PEHs applications, $H(\boldsymbol{\theta}, u)$ represents a Frequency Response Function (FRF), where $\boldsymbol{\theta}$ are electromechanical and geometric properties of the device and u the excitation frequency. A probabilistic model is then defined by assuming a predictive error e in $H(\boldsymbol{\theta}, u)$, commonly as additive by a zero mean and σ_n^2 variance Gaussian distribution $N(0, \sigma_n^2)$. Nevertheless, the adoption of this kind of error may lead to large variabilities in some sections of the predicted FRF, as demonstrated in [20]. Therefore, a multiplicative error is adopted, which leads to constant variability throughout the response:

$$h = H(\boldsymbol{\theta}, u) \cdot e \tag{2.3}$$

where h represents the probabilistic model response. Note that under a strictly positive output (as a FRF), this kind of error can be treated as additive if it is worked out between

the logarithms $\ln(h)$ and $\ln(H(\boldsymbol{\theta}, u))$. This leads to a lognormal distribution for e, and consequently, for h:

$$p(h|\boldsymbol{\theta}_{\mathrm{t}}, u) = \frac{1}{h\sigma_e\sqrt{2\pi}} \exp\left[-\frac{1}{2\sigma_e^2}(\ln(h) - \ln(H(\boldsymbol{\theta}, u)))^2\right] \tag{2.4}$$

where $\boldsymbol{\theta}_{\mathrm{t}}$ is the augmented parameter vector that ultimately defines the probabilistic model for h, which is composed of the model parameters $\boldsymbol{\theta}$ and the standard deviation of $\ln(e)$, i.e., σ_e. Now, let $\hat{\mathbf{U}} = \{\hat{u}_m; m = 1, \ldots, M\}$ and $\hat{\mathbf{H}} = \{\hat{h}_m; m = 1, \ldots, M\}$ denote vectors that represent M observations for the system input and output, respectively, and $\mathbf{D}$ the complete experimental data pair containing $\hat{\mathbf{U}}$ and $\hat{\mathbf{H}}$. If the observations are considered statistically independent, the likelihood of the observations $\hat{\mathbf{H}}$ is given by:

$$p(\hat{\mathbf{H}}|\boldsymbol{\theta}_{\mathrm{t}}, \hat{\mathbf{U}}) = \prod_{m=1}^{M} p(\hat{h}_m|\boldsymbol{\theta}_{\mathrm{t}}, \hat{u}_m) \tag{2.5}$$

which for the multiplicative error presented in Eq. (2.3) reduces to:

$$p(\hat{\mathbf{H}}|\boldsymbol{\theta}_{\mathrm{t}}, \hat{\mathbf{U}}) = \left(\frac{1}{\sigma_e\sqrt{2\pi}}\right)^M \left(\prod_{m=1}^{M} \frac{1}{\hat{h}_m}\right) \exp\left[-\frac{1}{2\sigma_e^2}\sum_{m=1}^{M}(\ln(\hat{h}_m) - \ln(H(\boldsymbol{\theta}, \hat{u}_m)))^2\right] \tag{2.6}$$

Then, with the definition of a prior probability density function $p(\boldsymbol{\theta}_{\mathrm{t}}|M_{cs})$ for the parameters, the Bayes rule is used to update them, to get a posterior description based on the experimental data $\mathbf{D}$:

$$p(\boldsymbol{\theta}_{\mathrm{t}}|\mathbf{D}, M_{cs}) = c^{-1}p(\mathbf{D}|\boldsymbol{\theta}_{\mathrm{t}}, M_{cs})p(\boldsymbol{\theta}_{\mathrm{t}}|M_{cs}) \tag{2.7}$$

where M_{cs} refers to the classical scheme model, $p(\mathbf{D}|\boldsymbol{\theta}_{\mathrm{t}}, M_{cs})$ is the likelihood function $p(\hat{\mathbf{H}}|\boldsymbol{\theta}_{\mathrm{t}}, \hat{\mathbf{U}})$ described above, and $c = P(\mathbf{D}|M_{cs})$ is a normalization constant called "evidence," which plays an essential role in the Bayesian model class selection procedure (discussed later). Lastly, $p(\boldsymbol{\theta}_{\mathrm{t}}|\mathbf{D}, M_{cs})$ is the updated PDF for $\boldsymbol{\theta}_{\mathrm{t}}$, which represents a posterior understanding of the model parameters given the experimental data $\mathbf{D}$. This distribution is called the posterior PDF.

Finding explicit analytical expressions for the posterior PDF is hardly reached due to the nonlinear relationship between H and $\boldsymbol{\theta}_{\mathrm{t}}$ introduced by the multiplicative error. It can be estimated, though, by drawing samples from it or by approximations of its modes. The latter are known as point estimates, where the Maximum A Posteriori (MAP) [14] estimate is found by (notation of M_{cs} is omitted for simplicity):

$$\boldsymbol{\theta}_{\mathrm{t}}^{MAP} = \arg\max \ \ln(p(\mathbf{D}|\boldsymbol{\theta}_{\mathrm{t}})p(\boldsymbol{\theta}_{\mathrm{t}})) \tag{2.8}$$

where the logarithm function is introduced for numerical reasons [14]. As noticed, this estimate focuses on the maximization of the numerator of Eq. (2.7), where prior information about parameters is considered. If the prior information is not included, the Maximum Likelihood Estimate (MLE) [33] is obtained:

$$\boldsymbol{\theta}_{\mathrm{t}}^{MLE} = \arg\max \ \ln p(\mathbf{D}|\boldsymbol{\theta}_{\mathrm{t}}) \tag{2.9}$$

When the posterior PDF happens to be heavily peaked on a single point, for posterior analysis (as discussed later), the point estimate can be used within the Laplace's asymptotic approximation to estimate the posterior integrals with good accuracy [15]. However, if this condition is not guaranteed, as it happens for PEHs [20], the approximation might be poor, yielding an erroneous account for system uncertainties. In this situation, full description of the posterior PDF needs to be used (e.g., by generating samples from it), allowing more reliable results.

2.2.2 Hierarchical Bayesian scheme

Now, let $\mathbf{D} = \{\mathbf{D}^i; i = 1, \ldots, N_i\}$ represent N_i different independent data pairs containing inputs $\{\hat{\mathbf{U}}^i; i = 1, \ldots, N_i\}$ and outputs $\{\hat{\mathbf{H}}^i; i = 1, \ldots, N_i\}$ of the system; each data pair defined by the parameters $\boldsymbol{\theta}_{\mathrm{t}}^i$. Under the hierarchical Bayesian scheme, each prior distribution for $\boldsymbol{\theta}_{\mathrm{t}}^i$, $p(\boldsymbol{\theta}_{\mathrm{t}}^i|\boldsymbol{\eta}, M_{hs})$, is parametrized by common hyperparameters $\boldsymbol{\eta}$, which introduces the hierarchy. In this sense, such hierarchical models are defined by two levels of parameters, the parameters for each data set $\boldsymbol{\theta}_{\mathrm{t}}^i$, and the hyperparameters $\boldsymbol{\eta}$. Compared to the classical Bayesian scheme, the hierarchy imposed allows the variation of the parameters across the data sets; and such variation can be described by the hyperparameters $\boldsymbol{\eta}$. Thus, using the Bayes theorem, the joint posterior distribution of the parameters $\{\boldsymbol{\theta}_{\mathrm{t}}^i; i = 1, \ldots, N_i\}$ and hyperparameters $\boldsymbol{\eta}$, is expressed as:

$$p(\{\boldsymbol{\theta}_{\mathrm{t}}^i; i = 1, \ldots, N_i\}, \boldsymbol{\eta}|\mathbf{D}, M_{hs}) = c^{-1} p(\boldsymbol{\eta}|M_{hs}) \prod_{i=1}^{N_i} p(\mathbf{D}^i|\boldsymbol{\theta}_{\mathrm{t}}^i, M_{hs}) p(\boldsymbol{\theta}_{\mathrm{t}}^i|\boldsymbol{\eta}, M_{hs}) \tag{2.10}$$

where M_{hs} refers to the hierarchical scheme model, $p(\boldsymbol{\eta}|M_{hs})$ is the prior distribution for the hyperparameters and $p(\mathbf{D}^i|\boldsymbol{\theta}_{\mathrm{t}}^i, M_{hs})$ is the likelihood function for each data set $\mathbf{D}^i$, whose expression is analogous to Eq. (2.6). Given the potentially large dimension of the posterior $p(\{\boldsymbol{\theta}_{\mathrm{t}}^i; i = 1, \ldots, N_i\}, \boldsymbol{\eta}|\mathbf{D}, M_{hs})$, the last equation is marginalized over the parameters $\boldsymbol{\theta}_{\mathrm{t}}^i$:

$$p(\boldsymbol{\eta}|\mathbf{D}, M_{hs}) = c^{-1} p(\boldsymbol{\eta}|M_{hs}) \prod_{i=1}^{N_i} p(\mathbf{D}^i|\boldsymbol{\eta}, M_{hs}) = c^{-1} p(\boldsymbol{\eta}|M_{hs}) p(\mathbf{D}|\boldsymbol{\eta}, M_{hs}) \tag{2.11}$$

where $c = P(\mathbf{D}|M_{hs})$ and $p(\boldsymbol{\eta}|\mathbf{D}, M_{hs})$ is the hyperparameters' posterior distribution, with:

$$p(\mathbf{D}^i|\boldsymbol{\eta}, M_{hs}) = \int p(\mathbf{D}^i|\boldsymbol{\theta}_{\mathrm{t}}^i, M_{hs}) p(\boldsymbol{\theta}_{\mathrm{t}}^i|\boldsymbol{\eta}, M_{hs}) d\boldsymbol{\theta}_{\mathrm{t}}^i \tag{2.12}$$

Different methods to estimate $p(\mathbf{D}^i|\boldsymbol{\eta}, M_{hs})$ are found in the literature. For example, for many data points, Sedehi et al. [24] used Laplace's asymptotic approximation for time series data. Wu et al. [28] proposed an importance sampling method with proposal distribution $p(\boldsymbol{\theta}_{\mathrm{t}}^i|\mathbf{D}^i, M_{cs})$, sampling with Transitional Markov Chain Monte Carlo (TMCMC) for each data set $\mathbf{D}^i$. In this work, the method proposed by Patsialis et al. [31] is employed, also relying on TMCMC. First, samples $\{\boldsymbol{\theta}_{\mathrm{t}}^{i(k)}; i = 1, \ldots, N_i, k = 1, \ldots, N_k\}$ from the likelihood function $p(\mathbf{D}^i|\boldsymbol{\theta}_{\mathrm{t}}^i, M_{hs})$ are obtained through TMCMC, by using a uniform prior distribution for $\boldsymbol{\theta}_{\mathrm{t}}^i \in [\boldsymbol{\theta}_{\mathrm{t}}^{\min}, \boldsymbol{\theta}_{\mathrm{t}}^{\max}]$. Then, Monte Carlo simulation is performed to estimate $p(\mathbf{D}^i|\boldsymbol{\eta}, M_{hs})$:

$$p(\mathbf{D}^i|\boldsymbol{\eta}, M_{hs}) \approx \frac{1}{N_k} \sum_{k=1}^{N_k} p(\boldsymbol{\theta}_{\mathrm{t}}^{i(k)}|\boldsymbol{\eta}, M_{hs}) \tag{2.13}$$

Finally, Eq. (2.13) is plugged into Eq. (2.11), which allows an expression for the posterior distribution of the hyperparameters $\boldsymbol{\eta}$:

$$p(\boldsymbol{\eta}|\mathbf{D}, M_{hs}) \approx c^{-1} p(\boldsymbol{\eta}|M_{hs}) \left[\prod_{i=1}^{N_i} \frac{1}{N_k} \sum_{k=1}^{N_k} p(\boldsymbol{\theta}_{\mathrm{t}}^{i(k)}|\boldsymbol{\eta}, M_{hs}) \right] \tag{2.14}$$

the samples of which can be generated using TMCMC, with prior $p(\boldsymbol{\eta}|M_{hs})$ and likelihood function the expression in the big brackets [31].

Under the assumption that the hyperparameters $\boldsymbol{\eta}$ can describe model parameter variations across the different data sets, the total probability theorem can be employed to compute the posterior distribution of the parameters under the hierarchical scheme $p(\boldsymbol{\theta}_{\mathrm{t}}|\mathbf{D}, M_{hs})$ [24]:

$$p(\boldsymbol{\theta}_{\mathrm{t}}|\mathbf{D}, M_{hs}) = \int p(\boldsymbol{\theta}_{\mathrm{t}}|\boldsymbol{\eta}, M_{hs}) p(\boldsymbol{\eta}|\mathbf{D}, M_{hs}) d\boldsymbol{\eta} \tag{2.15}$$

which can be estimated using the already available samples $\{\boldsymbol{\eta}^{(h)}; h = 1, \ldots, N_h\}$ obtained from Eq. (2.14), with Monte Carlo simulation:

$$p(\boldsymbol{\theta}_{\mathrm{t}}|\mathbf{D}, M_{hs}) \approx \frac{1}{N_h} \sum_{h=1}^{N_h} p(\boldsymbol{\theta}_{\mathrm{t}}|\boldsymbol{\eta}^{(h)}, M_{hs}) \tag{2.16}$$

If the distributions $p(\boldsymbol{\theta}_{\mathrm{t}}|\boldsymbol{\eta}^{(h)}, M_{hs})$ were established to be lognormal distributions with medians $\boldsymbol{\mu}$ and coefficients of variation $\mathbf{cov}$, in the logarithm space $\log(\boldsymbol{\theta}_{\mathrm{t}})$ they behave as Gaussian distributions. Thus, the sum of N_h Gaussian distributions is a Gaussian distribution with mean and covariance matrix [24]:

$$
\begin{aligned}
E[\log(\boldsymbol{\theta}_{\mathrm{t}})] &= \frac{1}{N_h}\sum_{h=1}^{N_h}\log\left(\boldsymbol{\mu}^{(h)}\right) \\
CoV[\log(\boldsymbol{\theta}_{\mathrm{t}})] &= \frac{1}{N_h}\sum_{h=1}^{N_h}\left(\log\left(\boldsymbol{\mu}^{(h)}\right)\log\left(\boldsymbol{\mu}^{(h)\mathrm{T}}\right)+\boldsymbol{\Sigma}^{(h)}\right) \\
&\quad -\frac{1}{N_h^2}\left(\sum_{h=1}^{N_h}\log\left(\boldsymbol{\mu}^{(h)}\right)\right)\left(\sum_{h=1}^{N_h}\log\left(\boldsymbol{\mu}^{(h)}\right)\right)^{\mathrm{T}}
\end{aligned}
\tag{2.17}
$$

where $\boldsymbol{\Sigma}^{(h)}$ are covariance matrices, calculated with the samples $\mathbf{cov}^{(h)}$.

Finally, $p(\boldsymbol{\theta}_{\mathrm{t}}|\mathbf{D}, M_{hs})$ can be used as an objective prior to update the parameters of each device. Thus, using Bayes rule:

$$
p(\boldsymbol{\theta}_{\mathrm{t}}^{i}|\mathbf{D}^{i}, M_{hs}) \propto p(\mathbf{D}^{i}|\boldsymbol{\theta}_{\mathrm{t}}^{i}, M_{hs})p(\boldsymbol{\theta}_{\mathrm{t}}|\mathbf{D}, M_{hs}) \tag{2.18}
$$

where $p(\mathbf{D}^{i}|\boldsymbol{\theta}_{\mathrm{t}}^{i}, M_{hs})$ is the likelihood function, whose expression is analogous to Eq. (2.6), and $p(\boldsymbol{\theta}_{\mathrm{t}}^{i}|\mathbf{D}^{i}, M_{hs})$ is the posterior distribution for each data set $\mathbf{D}^{i}$ using the objective prior that the hierarchical scheme offers.

Figure 2.1 shows the parameters' structure and dependence within the classical and hierarchical Bayesian schemes as a network.

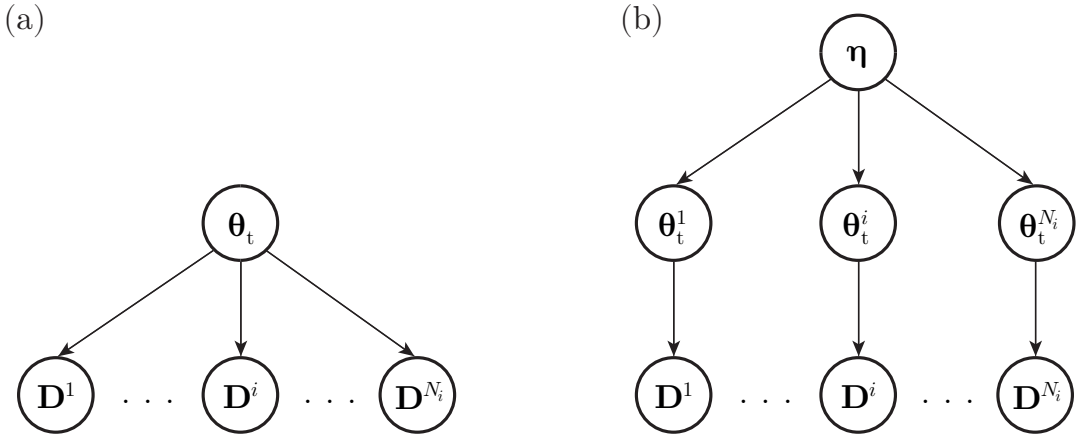

Figure 2.1: Graphical representations of the two Bayesian schemes: (a) Classical scheme and (b) Hierarchical scheme.

2.2.3 Model class selection

To further verify the preference for the hierarchical scheme/model over the classical scheme/-model, Bayesian model class selection will be used. Within the Bayesian inference framework,

data and model class selection can be used to select the best model among different model classes. Let $\{M_j; j = 1, \ldots, N\}$ represent the set of different model classes, with M_j denoting the jth model class. The posterior probability for each model class, conditioned on the experimental data $\mathbf{D}$, is obtained using Bayes' theorem:

$$P(M_j|\mathbf{D}) = \frac{P(\mathbf{D}|M_j)P(M_j)}{\sum_{j=1}^{N} P(\mathbf{D}|M_j)P(M_j)} \tag{2.19}$$

where $P(M_j)$ is the prior belief of adequacy of the jth model class, which is commonly taken as uniform across the set of models, i.e., $P(M_j) = 1/N$. The term $P(\mathbf{D}|M_j)$ is the evidence of each model class, which corresponds to the denominator of Eqs. (2.7) and (2.11), denoted by c. Notably, the estimation of $P(\mathbf{D}|M_j)$ is a by-product of the TMCMC algorithm. Finally, the posterior probability $P(M_j|\mathbf{D}) \propto P(\mathbf{D}|M_j)$ represents a logical criterion for selecting the most adequate model given experimental data, which imposes a principle of model parsimony [19]: model accuracy and model complexity are balanced out.

2.2.4 Prior and posterior predictive analyses

Depending on the information available, a predictive analysis for the system h can be performed. The deterministic prediction is straightforward as it only depends on the parameters' nominal values. In contrast, given the probabilistic description for the parameters within the Bayesian inference framework, a proper formulation for the prediction is required. Thus, the total probability theorem is employed to propagate the parameter uncertainties into the system output. For instance, the prior expected system output for a given input u, and model M_j, is:

$$E[h|u, M_j] = \int E[h|\boldsymbol{\theta}_{\mathrm{t}}, u, M_j]p(\boldsymbol{\theta}_{\mathrm{t}}|M_j)d\boldsymbol{\theta}_{\mathrm{t}} = \int H(\boldsymbol{\theta}, u)p(\boldsymbol{\theta}|M_j)d\boldsymbol{\theta} \tag{2.20}$$

where $E[h|\boldsymbol{\theta}_{\mathrm{t}}, u, M_j]$ is with respect to the whole probabilistic model, which includes the prediction error. However, under the usual assumption of unbiased predictions, $E[h|\boldsymbol{\theta}_{\mathrm{t}}, u, M_j] = H(\boldsymbol{\theta}, u)$, which explains the second equality of Eq. (2.20).

A confidence interval for the prediction can also be established, reflecting the probability that the model's prediction will lie inside that interval. For instance, for the prior distribution, the following probabilistic integral needs to be computed:

$$P(H \geq H_o|u, M_j) = \int I_f(\boldsymbol{\theta}, u)p(\boldsymbol{\theta}|M_j)d\boldsymbol{\theta} = P_o \tag{2.21}$$

where $I_f(\boldsymbol{\theta}, u)$ is the indicator function, $I_f(\boldsymbol{\theta}, u) = 1$ when $H(\boldsymbol{\theta}, u) \geq H_o$ and $I_f(\boldsymbol{\theta}, u) = 0$ otherwise. Thus, the threshold H_o is selected to get the desired probability bounds P_o^{low} and P_o^{up}, which will ultimately define the probability of the interval; commonly set to 90%. Note that in Eq. (2.21), the prediction error is not included since it is common only to propagate the model parameter uncertainties to analyze their impact on the system output. However,

the prediction error can be included by simply replacing $\boldsymbol{\theta}$ with $\boldsymbol{\theta}_{\mathrm{t}}$. Then, Eqs. (2.20) and (2.21) can be easily estimated using Monte Carlo simulation.

The same procedure can be performed for the posterior distribution, which only requires the replacement of $p(\boldsymbol{\theta}|M_j)$ with $p(\boldsymbol{\theta}|\mathbf{D}, M_j)$ in Eqs. (2.20) and (2.21):

$$E[h|u, \mathbf{D}, M_j] = \int E[h|\boldsymbol{\theta}_{\mathrm{t}}, u, M_j] p(\boldsymbol{\theta}_{\mathrm{t}}|\mathbf{D}, M_j) d\boldsymbol{\theta}_{\mathrm{t}} = \int H(\boldsymbol{\theta}, u) p(\boldsymbol{\theta}|\mathbf{D}, M_j) d\boldsymbol{\theta} \tag{2.22}$$

$$P(H \geq H_o|u, \mathbf{D}, M_j) = \int I_f(\boldsymbol{\theta}, u) p(\boldsymbol{\theta}|\mathbf{D}, M_j) d\boldsymbol{\theta} = P_o \tag{2.23}$$

which can be similarly estimated with Monte Carlo simulation using samples that follow the posterior $p(\boldsymbol{\theta}|\mathbf{D})$, obtained with TMCMC, for example.

Given the scope of this paper, please note that $\{M_j; j = cs, hs\}$. Proper explanations on how to compute $p(\boldsymbol{\theta}_{\mathrm{t}}|\mathbf{D}, M_{cs})$ and $p(\boldsymbol{\theta}_{\mathrm{t}}|\mathbf{D}, M_{hs})$ are presented later.

2.2.5 Transitional Markov chain Monte Carlo (TMCMC)

As the TMCMC method is extensively used in this work, a brief review is presented next. TMCMC algorithm [17, 34] is based on a sequential implementation of MCMC through auxiliary PDFs to finally converge to the posterior PDF $p(\boldsymbol{\theta}_{\mathrm{t}}|\mathbf{D})$. The transition defines the auxiliary PDFs $p_j(\boldsymbol{\theta}_{\mathrm{t}}|\mathbf{D}) \propto p(\mathbf{D}|\boldsymbol{\theta}_{\mathrm{t}})^{q_j} p(\boldsymbol{\theta}_{\mathrm{t}})$, with $\{q_j \in [0, 1]; j = 0, \ldots, n\}$. Thus, the transition is controlled by q_j, and for the extremes $q_0 = 0$ and $q_n = 1$, the densities correspond to $p_0(\boldsymbol{\theta}_{\mathrm{t}}|\mathbf{D}) \propto p(\boldsymbol{\theta}_{\mathrm{t}})$ and $p_n(\boldsymbol{\theta}_{\mathrm{t}}|\mathbf{D}) \propto p(\mathbf{D}|\boldsymbol{\theta}_{\mathrm{t}}) p(\boldsymbol{\theta}_{\mathrm{t}})$ respectively. The steps for obtaining N_s samples proportional to the posterior $p(\boldsymbol{\theta}_{\mathrm{t}}|\mathbf{D})$ through TMCMC are as follows:

Step 1: Let $\{\boldsymbol{\theta}_{\mathrm{t}}\}_j = \{\boldsymbol{\theta}^r_{\mathrm{t}(j)}; r = 1, \ldots, N_s\}$ represent a set of N_s samples from the j-level transition PDF $p_j(\boldsymbol{\theta}_{\mathrm{t}}|\mathbf{D})$, the exponent q_j is defined by setting the coefficient of variation of the expression $p_{j+1}(\boldsymbol{\theta}_{\mathrm{t}}|\mathbf{D})/p_j(\boldsymbol{\theta}_{\mathrm{t}}|\mathbf{D}) = p(\mathbf{D}|\boldsymbol{\theta}_{\mathrm{t}})^{q_{j+1}-q_j}$, commonly to 100%. If $q_j > 1$, then set $q_j = 1$. Note that the algorithm starts with N_s samples from $p_0(\boldsymbol{\theta}_{\mathrm{t}}|\mathbf{D}) \propto p(\boldsymbol{\theta}_{\mathrm{t}})$, which are easy to obtain since the prior PDF $p(\boldsymbol{\theta}_{\mathrm{t}})$ is free choice. Then, compute the samples plausibility weights with the evaluation of the quotient $w_{j+1}(\boldsymbol{\theta}_{\mathrm{t}}) = p_{j+1}(\boldsymbol{\theta}_{\mathrm{t}}|\mathbf{D})/p_j(\boldsymbol{\theta}_{\mathrm{t}}|\mathbf{D}) = p(\mathbf{D}|\boldsymbol{\theta}_{\mathrm{t}})^{q_{j+1}-q_j}$.

Step 2: Compute the mean of the weights:

$$\hat{S}_{j+1} = \frac{1}{N_s} \sum_{r=1}^{N_s} w_{j+1}(\boldsymbol{\theta}^r_{\mathrm{t}(j)}) \tag{2.24}$$

and the weighted sample mean and covariance matrix:

$$\bar{\boldsymbol{\theta}}_{j+1} = \frac{1}{\hat{S}_{j+1} N_s} \sum_{r=1}^{N_s} \boldsymbol{\theta}_{\mathrm{t}(j)}^{r} w_{j+1}(\boldsymbol{\theta}_{\mathrm{t}(j)}^{r})$$
$$\boldsymbol{\Sigma}_{j+1} = \frac{1}{\hat{S}_{j+1} N_s} \sum_{r=1}^{N_s} \left[w_{j+1}(\boldsymbol{\theta}_{\mathrm{t}(j)}^{r})(\boldsymbol{\theta}_{\mathrm{t}(j)}^{r} - \bar{\boldsymbol{\theta}}_{j+1})(\boldsymbol{\theta}_{\mathrm{t}(j)}^{r} - \bar{\boldsymbol{\theta}}_{j+1})^{\mathrm{T}} \right] \tag{2.25}$$

Step 3: According to the computed weights w_{j+1}, resample N_{t} samples with replacement from the set $\{\boldsymbol{\theta}_{\mathrm{t}}\}_j$. These ultimately correspond to samples from $p_{j+1}(\boldsymbol{\theta}_{\mathrm{t}}|\mathbf{D})$.

Step 4: From each $c^{th}(c = 1, \ldots, N_{\mathrm{t}})$ sample, start independent Markov chains, repeating random walk moves using $\beta^2 \boldsymbol{\Sigma}_{j+1}$, where β is a scaling factor typically set to 0.2 [17]. For the p^{th} random walk move, generate a candidate $\tilde{\boldsymbol{\theta}}_{\mathrm{t}(c)}^{r}$ from a gaussian proposal centered at $\boldsymbol{\theta}_{\mathrm{t}(c)}^{r-1}$ and covariance matrix $\beta^2 \boldsymbol{\Sigma}_{\boldsymbol{j+1}}$. Generate a sample u from an uniform distribution [0,1] and set $\boldsymbol{\theta}_{\mathrm{t}(c)}^{r} = \tilde{\boldsymbol{\theta}}_{\mathrm{t}(c)}^{r}$ if the following condition is satisfied:

$$\frac{p_{j+1}(\tilde{\boldsymbol{\theta}}_{\mathrm{t}(c)}^{r}|\mathbf{D})}{p_{j+1}(\boldsymbol{\theta}_{\mathrm{t}(c)}^{r}|\mathbf{D})} \geq u \tag{2.26}$$

otherwise set $\boldsymbol{\theta}_{\mathrm{t}(c)}^{r} = \boldsymbol{\theta}_{\mathrm{t}(c)}^{r-1}$. After finishing the random walk moves for each chain, combine the samples to obtain N_s samples $\{\boldsymbol{\theta}_{\mathrm{t}}\}_{j+1}$ that are proportional to the transitional distribution $p_{j+1}(\boldsymbol{\theta}_{\mathrm{t}}|\mathbf{D})$.

The steps are repeated until $q_j = 1$. Finally, the algorithm provides an estimation for the evidence, given by:

$$P(\mathbf{D}|M_j) = \prod_{j=0}^{n-1} \hat{S}_{j+1} \tag{2.27}$$

Chapter 3

PEH's uncertainties

3.1 Model parameters uncertainties and prior probability density function for PEHs

According to [13], typical dispersions related to geometric and electromechanical properties of PEHs can reach values of 30% (respect to nominal values). These variations are mainly attributed to manufacturing process imperfections, which critically affect PEHs response functions [12]. Particularly, geometric characteristics present the lowest dispersions, reaching values of 5% of variation. In contrast, electromechanical properties present the greatest, with variations up to 30% [13]. Some manufacturers do not even report substructure mechanical properties, increasing even more the system uncertainties.

A set of commercial bimorph PEHs were studied in this work, which had layers of piezoelectric material ZT-5X45 bonded to a carbon fiber's substructure layer. The nominal characteristics of the devices are presented in Table 3.1. Based on this available information, a prior PDF $p(\boldsymbol{\theta}_t|M_{cs})$ for the model parameters is constructed. For continuity and consistency with [20, 21, 22], it is decided to define the prior distribution as a multivariate lognormal distribution with a median equal to the nominal values, and coefficients of variation (cov) of 5% for the geometric characteristics and 30% for the electromechanical properties. Since there is no available information about the substructure's properties, its elastic modulus and density are taken equal to the piezoelectric layer's properties with a coefficient of variation of 100%.

Note that the selection of a lognormal distribution is supported by the maximum information entropy principle [35] and also accounts for the positive nature of the model parameters.

3.2 Experimental identification of multiple PEHs

FRF observations from nine PEHs, all of them sharing the nominal characteristics presented in Table 3.1 were available. The data was acquired by Peralta et al. [12] and the procedure used allows the noise-free identification of the FRF at several excitation frequencies. Hence,

Table 3.1: Nominal characteristics of the bimorph PEHs studied. The prior model is also presented corresponding to a lognormal distribution with the given median and coefficient of variation (cov).

Parameter	Nominal	Prior	
		Median	cov
ζ	N/R	0.017	30%
s_{11}^E [pN^{-1} m^2]	16.4	16.4	30%
$-d_{31}$ [pC N^{-1}]	320	320	30%
$\varepsilon_{33}^T/\varepsilon_0$	4500	4500	30%
ρ_p [kg/m^3]	7400	7400	30%
ρ_s [kg/m^3]	N/R	7400	100%
E_s [GPa]	N/R	61	100%
L [mm]	40	40	5%
b [mm]	10	10	5%
h_s [mm]	0.234	0.234	5%
h_p [mm]	0.248	0.248	5%

N/R: Not reported by the manufacturer

$\varepsilon_0 = 8.854\times10^{-12}$ [F m^{-1}]

for each device $\{i = 1, \ldots, 9\}$, frequency excitation data $\hat{\mathbf{W}} = \{\hat{\omega}_m; m = 1, \ldots, M\}$ and FRF data $\hat{\mathbf{H}} = \{\hat{h}_m; m = 1, \ldots, M\}$ are available, representing the input and the output of the system, respectively, and ultimately defining each device's data set $\mathbf{D}^i$ and $\mathbf{D} = \{\mathbf{D}^i; i = 1, \ldots, 9\}$. The experimental FRFs from the nine PEHs, along with the deterministic prediction, are shown in Figure 3.1(a). The deterministic prediction was obtained with the nominal values presented in Table 3.1, and for those not reported (N/R) parameters, they were taken equal to the median of the prior PDF. As noticed, the nine devices present dissimilar behaviors, mainly attributed to variations in the electromechanical properties, as discussed before. In this sense, the experimental identification of only one device may not represent the behavior of the whole group [12]. Also, note that the deterministic prediction given by the solid black line showed a poor data fit across the nine PEHs, overestimating their natural frequencies.

A prior predictive analysis was also performed, with the prior distribution $p(\boldsymbol{\theta}_t|M_{cs})$ defined in the section before. Following Section 2.2.4 (estimating Eqs. (2.20) and (2.21) by applying a Direct Monte Carlo with 6000 samples), the probabilistic prediction is defined by a mean prediction and a 90% confidence band, shown in Figure 3.1(b). A significant dispersion band was obtained, which enclosed most of the data from the nine PEHs. Nevertheless, the large dispersion obtained seems to overrate the actual dispersions present in the group

of harvesters, as also obtained by Peralta et al. [12]. Similar to the nominal prediction, the prior mean prediction also overestimated the harvesters' natural frequency.

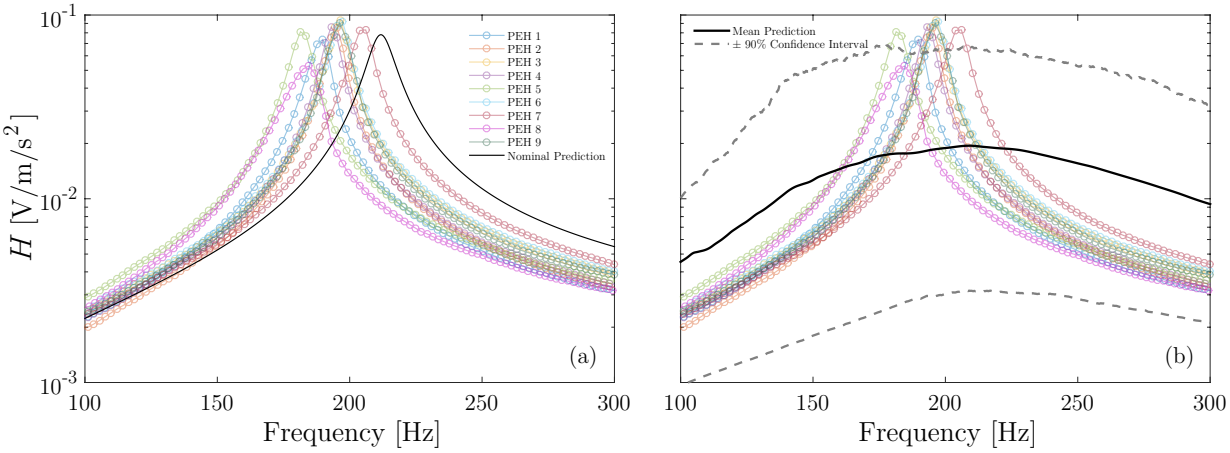

Figure 3.1: (a) Nominal prediction and (b) Prior stochastic prediction representing a 90% confidence interval. In both cases experimental FRFs for the 9 PEHs are presented in circles. The prior distribution used in (b) is adopted based on the information given by the manufacturer. The nominal estimation is biased and the uncertainties described through the prior in overestimated.

Chapter 4

Bayesian inference on PEHs

In this Chapter, the Bayesian inference framework is applied to the nine devices mentioned above. The classical and hierarchical Bayesian schemes for model parameter updating are implemented for individual and multiple devices. Posterior predictive analyses and model class selection procedures are conducted to illustrate their differences.

4.1 Model parameter updating

4.1.1 Classical Bayesian scheme

The classical Bayesian scheme detailed in Section 2.1.1 is applied for the Bayesian inference of the parameters for the nine devices. The prior distribution for the model parameters corresponded to the lognormal distribution detailed in Table 3.1. The prediction error standard deviation σ_e was also considered uncertain, with a prior lognormal distribution centered at 0.1 and 400% of cov, accounting for the poor prior information on this error. This finally defines the prior model $p(\boldsymbol{\theta}_\mathrm{t}|M_{cs})$ for all the parameters.

Firstly, the Bayesian scheme was used to update each device individually. Thus, each data set $\mathbf{D}^i$ was used to identify the parameters $\boldsymbol{\theta}_\mathrm{t}^i$, as Peralta et al. [20] did for a given device:

$$p(\boldsymbol{\theta}_\mathrm{t}^i|\mathbf{D}^i, M_{cs}) \propto p(\mathbf{D}^i|\boldsymbol{\theta}_\mathrm{t}^i, M_{cs})p(\boldsymbol{\theta}_\mathrm{t}|M_{cs}) \tag{4.1}$$

Note that the same prior distribution $p(\boldsymbol{\theta}_\mathrm{t}|M_{cs})$ was employed in each updating process. The updated parameters (obtained via TMCMC) from each data set varied between them, accounting for each device's dissimilar behavior. Consequently, the samples from each posterior distribution $p(\boldsymbol{\theta}_\mathrm{t}^i|\mathbf{D}^i, M_{cs})$ offered an excellent fit to the correspondent device, but not for the others. Figure 4.1 shows the robust posterior predictions generated with each device's updated parameters, where the colored areas represent a 90% confidence interval. Only PEHs properties and characteristics were propagated. The narrow robust predictions are explained by the strong correlations found in some model parameters, which offset the dispersions found, as also obtained by Peralta et al. [20]. The pair $s_{11}^E - d_{31}$ was the most

repeated, reaching coefficients of correlation higher than 0.85.

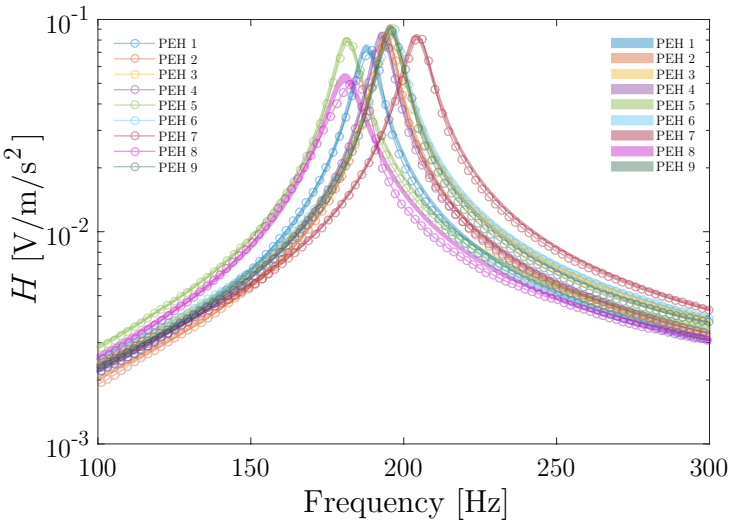

Figure 4.1: Robust posterior predictions generated by the updated model parameters of each device adopting a classical Bayesian approach. The colored bands represent a 90% confidence interval. Experimental FRFs for the 9 PEHs are presented in circles. It is observed small dispersion in each PEH.

In order to get a general description for all the devices, it is straightforward to compute the median and coefficient of variation of all the samples (combining samples obtained from the posterior distribution of each device), which are reported in Table 4.1. In addition, the relative absolute differences with the nominal values listed in Table 3.1 are also reported. Among the PEHs properties, the larger difference was obtained in the permittivity constant ε_{33}^T, whilst the smallest ($<$3%) were reported in geometric characteristics and ρ_p. The variability obtained of the model parameters was lower than the initial; only geometric characteristics and E_s remained close to their initial coefficient of variation.

A posterior predictive analysis was performed for the combined results as well, where only PEHs properties and characteristics were propagated. For each model parameter, a lognormal distribution was assumed, centered at the samples' median and coefficients of variation the values reported in Table 4.1. Two cases were explored corresponding to considering or not the correlations found. For the first case, a diagonal covariance matrix was considered, and for the second one, the covariance matrix was directly computed from all samples combined. The mean prediction and 90% confidence interval for each case are shown in Figure 4.2. For the first one, the mean prediction estimated well the mean natural frequency of the devices but presented a wide 90% confidence interval band, slightly improving the prior distribution's prediction (Figure 3.1(b)). In contrast, when the correlations between model parameters are considered, a much better prediction is reached, however, the FRF dispersion is overestimated. Besides, the method used to reach it was not rigorous, as it consists of the raw combination of samples obtained separately with the Bayesian updating. The results demonstrate the impact of the model parameter correlations within the classical Bayesian scheme for PEHs applications.

The study continued with the parameter updating using the entire data set $\mathbf{D}$, which

contains the FRF observations of all the devices. Samples from the posterior distribution $p(\boldsymbol{\theta}_t|\mathbf{D}, M_{cs})$, given by Eq. (2.7), were obtained through TMCMC. Table 4.2 shows the updated medians and cov of the parameters and the relative absolute differences with the values showed in Table 4.1. Among the PEH properties, no major differences were obtained, with the highest in the damping ratio ζ (77%). In contrast, the prediction error σ_e presented a large increase in its value (1052%), reporting disagreement with the experimental data.

Table 4.1: Medians and coefficients of variation obtained combining samples of the updated model parameters of each device adopting a classical Bayesian approach. The relative absolute differences respect to nominal values are reported as percentage in parenthesis.

Parameter	Median	cov
ζ	0.0147 (14%)	25%
s_{11}^E [pN^{-1} m^2]	17.5 (7%)	19%
$-d_{31}$ [pC N^{-1}]	284.4 (11%)	18%
$\varepsilon_{33}^T/\varepsilon_0$	10009 (122%)	11%
ρ_p [kg/m^3]	7603 (3%)	26%
ρ_s [kg/m^3]	7014 (5%)	73%
E_s [GPa]	63.9 (5%)	110%
L [mm]	40.68 (2%)	4%
b [mm]	10.24 (2%)	5%
h_s [mm]	0.233 (<1%)	5%
h_p [mm]	0.243 (2%)	5%
σ_e	0.023(77%)	47%

If compared to Table 4.1, the dispersions remained almost equal, where only ζ presented a difference of more than six percentage points. Strong correlations between model parameters were also reported. Particularly, the group of model parameters $\zeta - s_{11}^E - d_{31} - \rho_s$ were highly correlated, where the pair $s_{11}^E - d_{31}$ presented a correlation coefficient of 0.93. Figure 4.3 shows the posterior samples strongly correlated ($|\rho| > 0.5$). These correlations are consistent with previous analyses found in [20, 22].

To further investigate the effects of the features mentioned before, a posterior predictive analysis was carried out. It was performed for two cases: with only PEHs properties and characteristics, and then including the prediction error σ_e. Figure 4.4 shows the mean prediction and the 90% confidence interval found for the two cases mentioned, along with the nine devices' experimental data. As noted, the mean prediction is equal for both cases, which estimates well the mean natural frequency of the devices. Nevertheless, the confidence interval widths differ noticeably. When only considering model parameters uncertainties, the interval obtained is very narrow and does not enclose the devices' experimental data correctly. The very narrow interval is explained again by the strong correlations obtained,

which compensate for the high dispersion found in some model parameters. This aspect has been thoroughly addressed by Peralta et al. [20], which pointed out that there is a significant trade-off between the large coefficients of variation and strong correlations found in PEHs model parameters. It was also demonstrated that the system is globally identifiable. Therefore, the posterior distribution does present regions that offer almost the same likelihood value of the MAP estimate, yielding very similar FRF predictions. Otherwise, when the prediction error σ_e is considered, a much wider confidence interval is encountered, which encloses in a better way the experimental data. As the variance of the devices is mainly attributed to model parameter variations, these results are unrealistic. The erroneous account for the system uncertainties was expected, as it has been reported that the classical scheme commonly puts the system uncertainties (model error and parameters variability) in the prediction error [23, 26], as was discussed in the introduction.

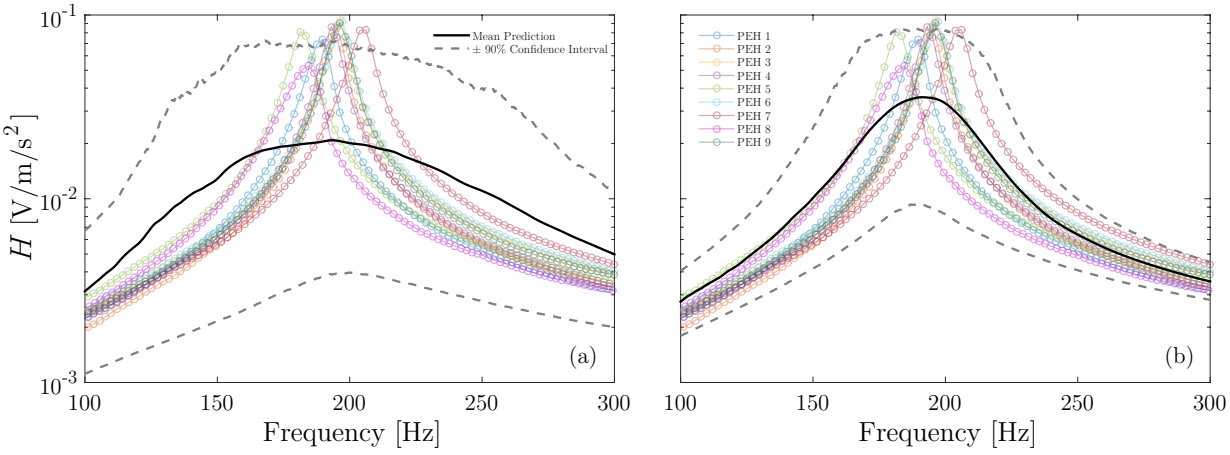

Figure 4.2: Robust posterior predictions with a confidence interval of 90%, obtained combining the updated model parameters of each device adopting a classical Bayesian approach (prediction error is not included). (a) Ignoring correlations and (b) incorporating correlation identified in the posterior distribution of each device. Experimental FRFs for the 9 PEHs are presented in circles. The predicted FRF dispersion is overestimated.

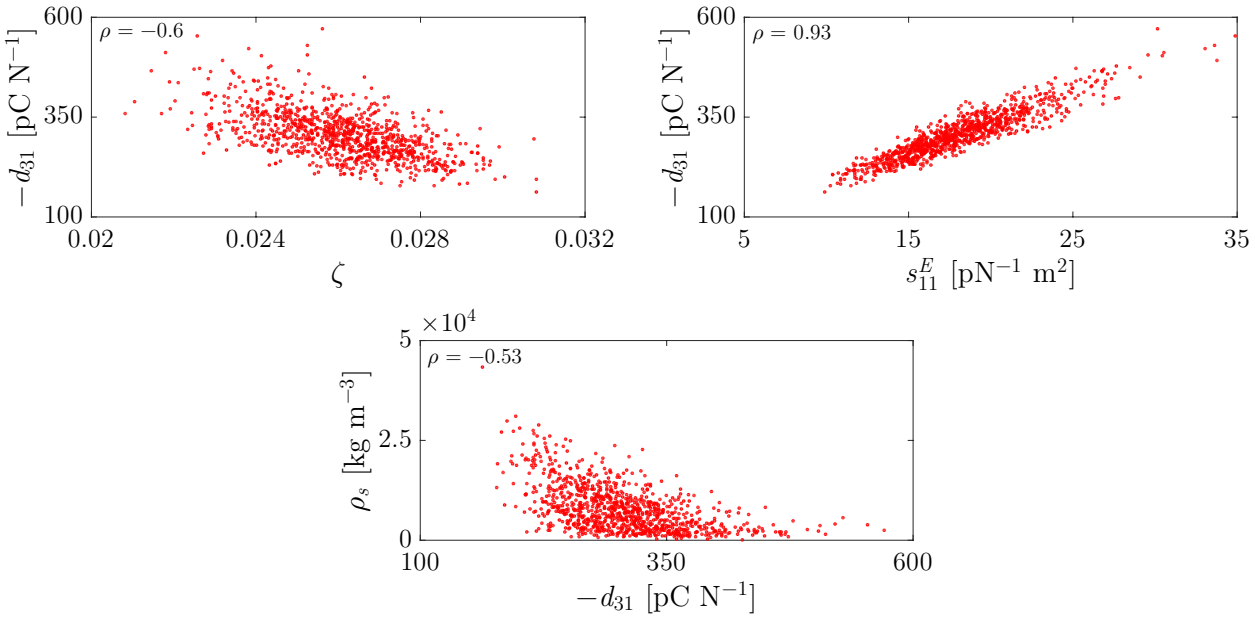

Figure 4.3: Posterior samples with largest correlation coefficients ($|\rho| > 0.5$), obtained combining the experimental FRF to update model parameters of a single predictive model adopting a classical Bayesian scheme. Correlation coefficients are indicated in the top left corner.

Table 4.2: Median and coefficient of variation of each model parameter updated using the full data set **D** on a classical Bayesian approach. The relative absolute differences with the median values of Table 4.1 are reported as percentage in parenthesis.

Parameter	Posterior	
	Median	cov
ζ	0.026 (77%)	6%
s_{11}^E [pN^{-1} m^2]	17.6 (<1%)	19%
$-d_{31}$ [pC N^{-1}]	300.3 (5%)	19%
$\varepsilon_{33}^T/\varepsilon_0$	9443 (6%)	15%
ρ_p [kg/m^3]	7402 (3%)	26%
ρ_s [kg/m^3]	6437 (8%)	73%
E_s [GPa]	63.9 (<1%)	103%
L [mm]	41.08 (1%)	5%
b [mm]	10.11 (1%)	5%
h_s [mm]	0.232 (1%)	5%
h_p [mm]	0.241 (1%)	5%
σ_e	0.265 (1052%)	2%

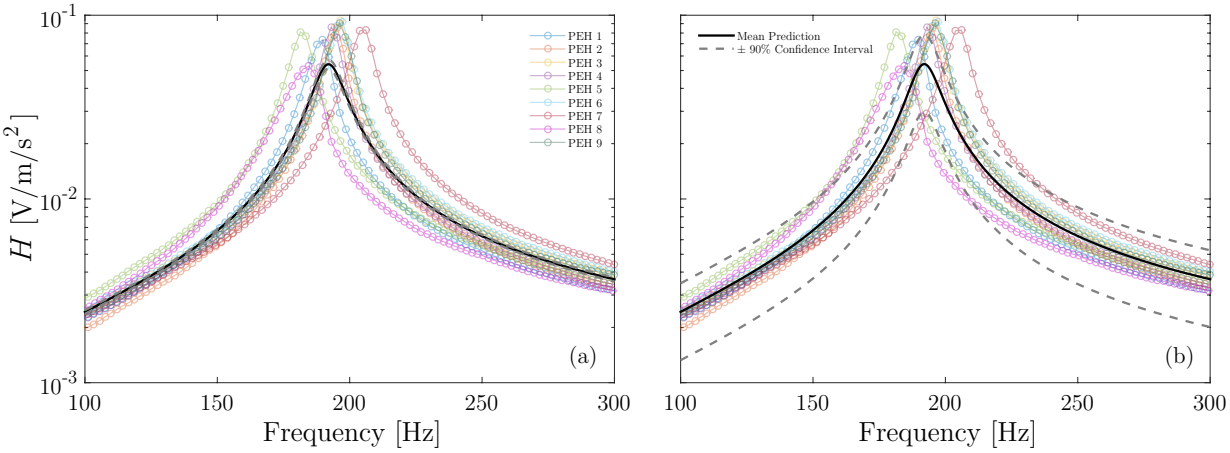

Figure 4.4: Predicted FRF with a confidence interval of 90%, obtained combining the experimental FRF to update model parameters of a single predictive model adopting a classical Bayesian scheme. (a) only model parameters uncertainties considered. (b) prediction error also considered. Experimental FRFs for the 9 PEHs are presented in circles. The model parameters uncertainties (excluding the predictive error) underestimate the FRF dispersion.

4.1.2 Hierarchical Bayesian scheme

Given the unrealistic account for model parameter uncertainties obtained with the classical Bayesian scheme, the hierarchical approach is conducted. Now, each harvester data set $\mathbf{D}^i$ is treated independently and is defined by model parameters $\boldsymbol{\theta}_{\mathrm{t}}^i$. The hierarchy, as mentioned before, is established by parameterizing the prior distribution of each data sets' parameters, leading to $p(\boldsymbol{\theta}_{\mathrm{t}}^i|\boldsymbol{\eta}, M_{hs})$. Given that the parameters prior PDF was selected to be a multivariate uncorrelated lognormal distribution, defined by medians $\boldsymbol{\mu}$ and coefficient of variations $\mathbf{cov}$, the hyperparameters $\boldsymbol{\eta}$ consist of the set $[\boldsymbol{\mu}\ \mathbf{cov}]$. The prediction error σ_e was also parameterized, as the FRF data from the nine harvesters were acquired under the same experimental setup [12], which ensures noise-free measurements. In this sense, the prediction error is not expected to present high variations across the experiments.

The implementation of the hierarchical Bayesian scheme was then performed following the procedure detailed in Section 2.2.2. Thus, it started with obtaining samples from the likelihood function of each data set $p(\mathbf{D}^i|\boldsymbol{\theta}_{\mathrm{t}}^i, M_{hs})$, which allows the estimation of the integrals $\{p(\mathbf{D}^i|\boldsymbol{\eta}, M_{hs}); i = 1, \ldots, 9\}$, given by Eq. (2.13). The samples were obtained using a uniform prior distribution for the parameters $\boldsymbol{\theta}_{\mathrm{t}}^i \in [\boldsymbol{\theta}_{\mathrm{t}}^{\min}, \boldsymbol{\theta}_{\mathrm{t}}^{\max}]$, where the limits $\boldsymbol{\theta}_{\mathrm{t}}^{\min}$ and $\boldsymbol{\theta}_{\mathrm{t}}^{\max}$ were selected to be the prior medians ± two prior standard deviations, whose values are shown in Table 3.1. These limits would represent the physical space where the uncertain parameters $\boldsymbol{\theta}_{\mathrm{t}}^i$ may lay.

Then, with Eq. (2.14), samples $\{\boldsymbol{\eta}^{(h)}; h = 1, \ldots, N_h\}$ from $p(\boldsymbol{\eta}|\mathbf{D}, M_{hs})$, which contain the medians $\boldsymbol{\mu}^{(h)}$ and coefficients of variations $\mathbf{cov}^{(h)}$, were obtained through TMCMC with a uniform prior distribution $p(\boldsymbol{\eta}|M_{hs})$: the medians $\boldsymbol{\mu}$ were bounded by the same limits $\boldsymbol{\theta}_{\mathrm{t}}^{\min}$ and $\boldsymbol{\theta}_{\mathrm{t}}^{\max}$ mentioned before, and the coefficients of variations $\mathbf{cov}$ were bounded between 0.001% and 500%. The posterior samples of the hyperparameters $\boldsymbol{\eta}^{(h)}$ are shown in Figure 4.5, corresponding to scatter plots for the medians $\boldsymbol{\mu}^{(h)}$ and coefficients of variation $\mathbf{cov}^{(h)}$ of

each model parameter.

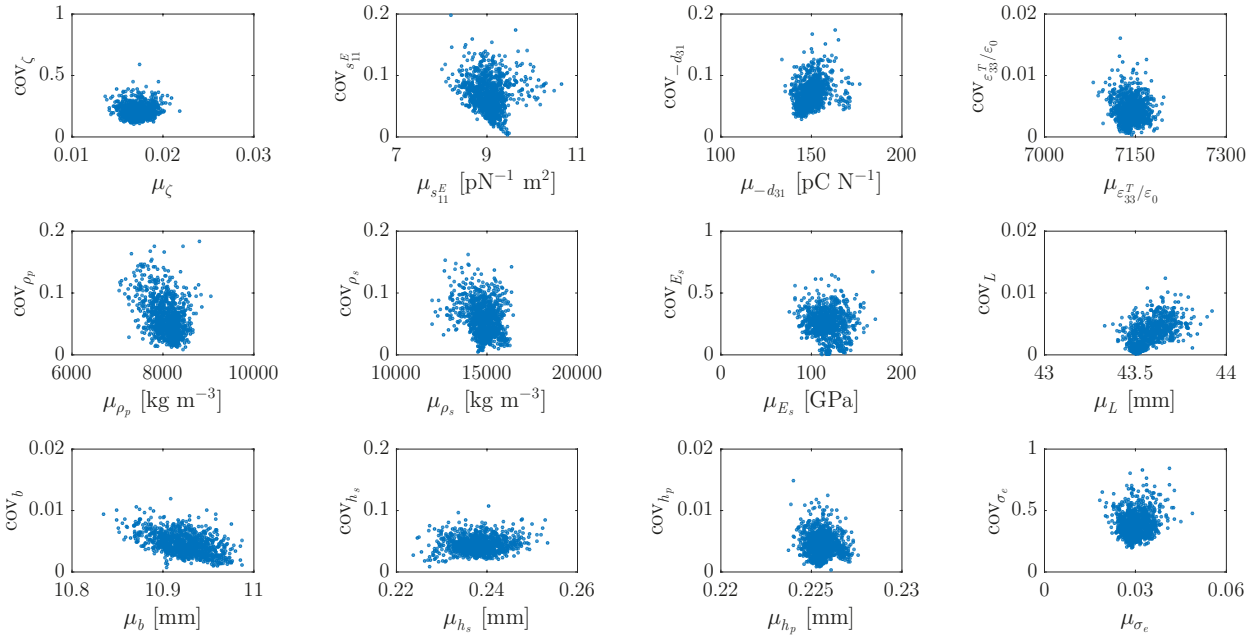

Figure 4.5: Samples from $p(\boldsymbol{\eta}|\mathbf{D}, M_{hs})$ obtained through TMCMC. These samples correspond to the posterior distribution of the hyper-parameters.

Then, using Eq. (2.17) the medians and dispersions of $p(\boldsymbol{\theta}_t|\mathbf{D}, M_{hs})$ were calculated, which are shown in Table 4.3. Significant differences with the values obtained with the classical scheme are observed, demonstrating the impact of introducing the prior distribution $p(\boldsymbol{\theta}_t|M_{cs})$. The parameter σ_e, associated with the prediction error, showed a huge decrease in its value, revealing the different structure of the hierarchical scheme. Also, most of the PEHs properties and characteristics showed a decrease in their dispersions compared to the ones obtained within the classical scheme (Table 4.2); only ζ reported an increase of sixteen percentual points. Given the analytical posterior distribution $p(\boldsymbol{\theta}_t|\mathbf{D}, M_{hs})$ the hierarchical setting offers, contour plots of the joint distribution of parameter pairs are shown in Figure 4.6. In contrast with the classical scheme, no correlations between parameters are obtained under the hierarchical approach, given that correlation coefficients are not considered in the hyperparameter vector $\boldsymbol{\eta}$.

A posterior predictive analysis is performed to propagate the uncertainties $p(\boldsymbol{\theta}_t|\mathbf{D}, M_{hs})$ in the FRFs. Here, two cases are analyzed: considering and not the prediction error, yielding to the robust predictions shown in Figure 4.7. The figure shows the mean FRF in solid black line and experimental FRF of each PEH in circles. Additionally, the 90% confidence intervals are also included, where the red dotted line incorporates the prediction error while the gray dotted line excludes it. Practically no difference between the predictions (with and without the prediction error) is obtained due to the small value obtained for σ_e. Contrary to the classical scheme's prediction (Figure 4.4), the hierarchical method correctly accounts for the variability across the nine devices rigorously. In conclusion, the hierarchical approach accurately bounds the entire FRF data set. Therefore, a good estimation for the mean natural frequency and highest voltage response is reached.

Table 4.3: Updated medians and covs of $p(\boldsymbol{\theta}_t|\mathbf{D}, M_{hs})$ given by the hierarchical scheme. The relative absolute differences with the classical scheme are reported as percentage in parenthesis.

Parameter	Posterior	
	Median	cov
ζ	0.0172 (34%)	22%
s_{11}^E [pN^{-1} m^2]	9.1 (49%)	8%
$-d_{31}$ [pC N^{-1}]	150.29 (50%)	8%
$\varepsilon_{33}^T/\varepsilon_0$	7144 (24%)	1%
ρ_p [kg/m^3]	8035 (9%)	8%
ρ_s [kg/m^3]	14801 (130%)	8%
E_s [GPa]	116.6 (82%)	29%
L [mm]	43.57 (6%)	<1%
b [mm]	10.92 (8%)	1%
h_s [mm]	0.238 (3%)	5%
h_p [mm]	0.226 (6%)	1%
σ_e	0.030 (89%)	42%

To further investigate the differences between the classical and hierarchical approach, the marginalized histograms of the posterior distributions, $p(\boldsymbol{\theta}_t|\mathbf{D}, M_{cs})$ and $p(\boldsymbol{\theta}_t|\mathbf{D}, M_{hs})$, respectively, are compared in Figure 4.8. Blue histograms correspond to the classical scheme, while the red ones correspond to the hierarchical scheme. As noted, lower dispersions were obtained with the hierarchical scheme, where some parameters, such as ε_{33}^T, L, b and h_p presented values of 1%. This behavior was not expected since it is common to obtain larger model parameter dispersions within the hierarchical scheme compared to the classical one. The behavior is explained by the critical role that model parameter correlations play in the parameter uncertainty quantification within the classical scheme, discussed in Section 4.1. As the hierarchical scheme was structured as uncorrelated, the trade-off effect vanishes, yielding the decrease in model parameters dispersions. Thus, the hierarchical and classical schemes are not compared under the same assumptions. It should be noted that if model parameter correlation coefficients were considered within the hierarchical scheme, a 90-dimensional hyperparameter vector is engendered, where alternative identification methods should be explored due to the significant computational cost involved. Secondly is the different assessment of the prediction error σ_e, which is manifested on its widely separated histograms. While the classical scheme puts most of the variability of the data sets on the prediction error, critically overestimating it, the hierarchical scheme puts it on model parameter uncertainties.

Further insight can be obtained if the prediction given by the MAP values of each scheme are contrasted against the experimental data. For comparison, a similar procedure to [22]

is performed. Thus, MAP predictions are presented into the physical space and also in a normalized FRF space, defined by the following axes: $r = \omega/\omega_o$ and $H_N = H/H_o$, where ω_o and H_o are the natural frequency and its corresponding FRF amplitude. The transformation into the normalized FRF space is supported by the fact that its shape is independent of the value of the natural frequency and the peak of amplitude. Figure 4.9 shows the predictions provided by the MAP values of each scheme in both spaces defined before, along with the experimental FRFs. Classical scheme MAP prediction is presented in a red solid line, while the hierarchical in a blue. It is observed that the curve obtained with the classical scheme has a poor agreement with the natural frequency and the maximum FRF amplitude. In contrast, the prediction provided by the hierarchical scheme has good agreement with both values. On the other hand, when the FRF shape is considered, Figure 4.9(b) reveals a poor agreement between the MAP curve of the classical scheme and the experimental data since its prediction is above the data points. In contrast, MAP prediction from the hierarchical scheme presents an appropriate fit. In this line, the proposed hierarchical scheme significantly improves the results obtained in [22] without manipulating experimental data.

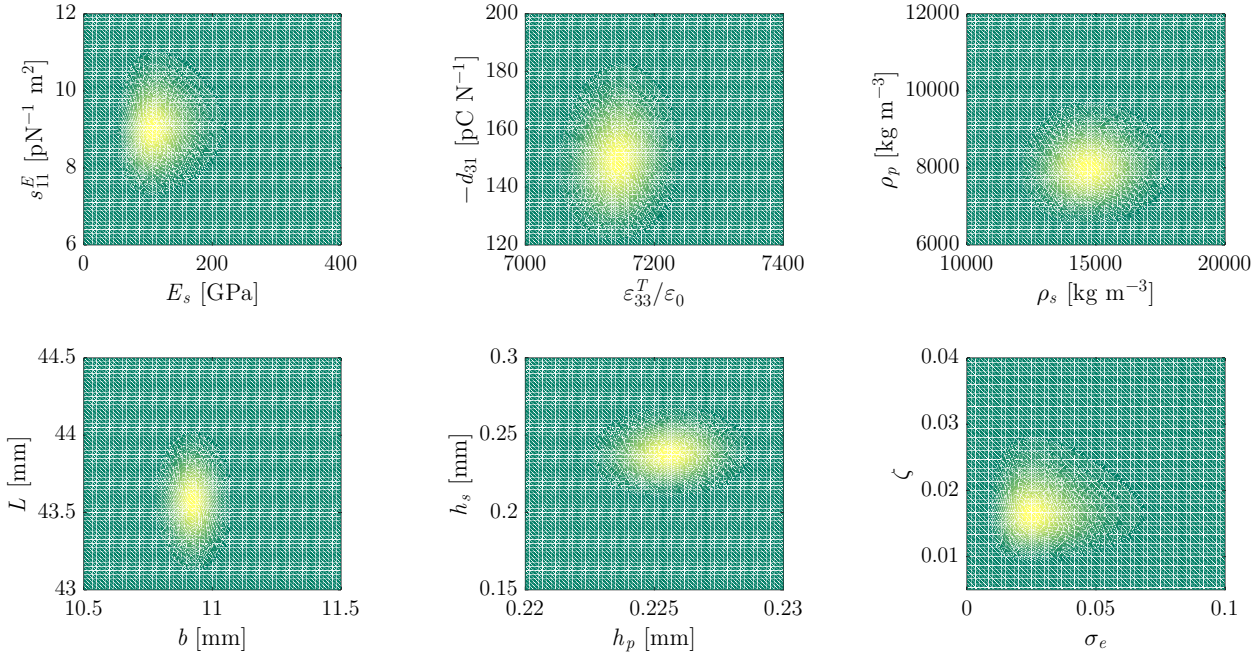

Figure 4.6: Joint posterior distribution of model parameter pairs given by the hierarchical approach. The distribution corresponds to the approximation of $p(\boldsymbol{\theta}_{\mathrm{t}}|\mathbf{D}, M_{hs})$ made by a Monte Carlo approach in Eq. (2.16). This PDF is considered as the underlaying distribution of model parameters of the group of PEHs.

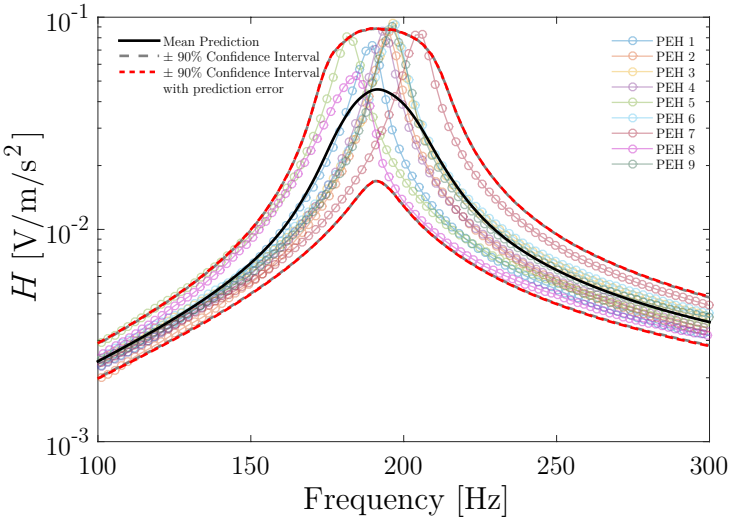

Figure 4.7: Predicted FRF with a confidence interval of 90% given the $p(\boldsymbol{\theta}_t|\mathbf{D}, M_{hs})$ identified by the hierarchical Bayesian scheme. Experimental FRFs for the 9 PEHs are presented in circles. The model parameters uncertainties (excluding the prediction error) predict a FRF dispersion in agreement with the experimental observations.

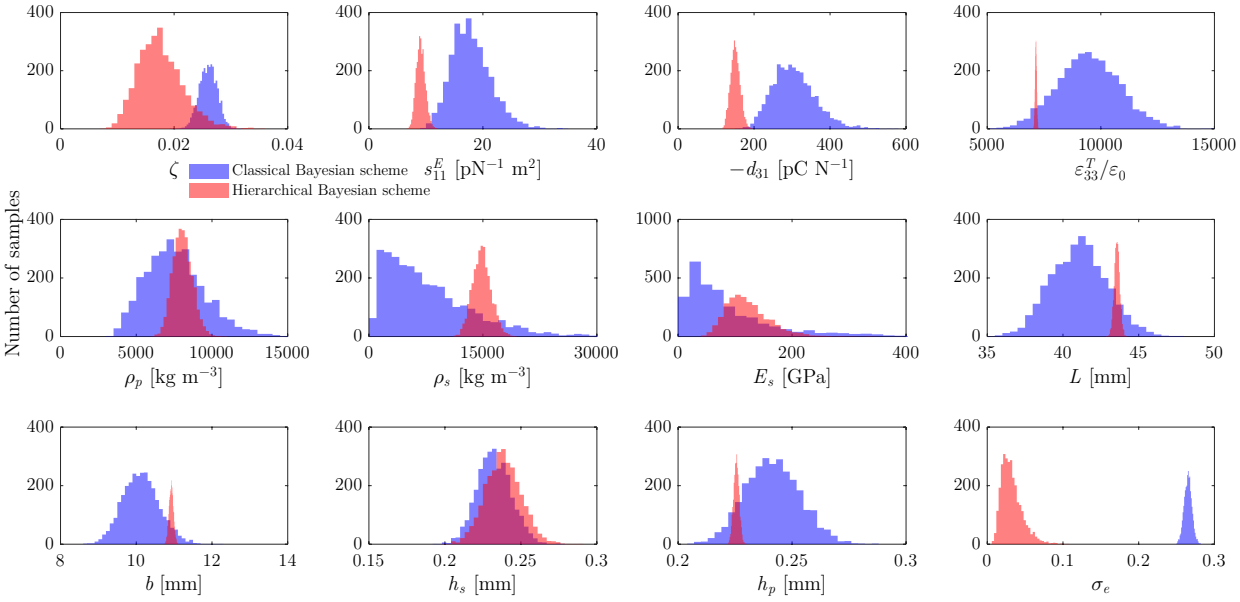

Figure 4.8: Marginalized model parameter histograms of the posterior distribution for the group of harvesters obtained with the classical (blue) and hierarchical (red) approaches. Samples in color blue were used to obtain Fig. 4.4 while samples in color red were used to obtain Fig. 4.7. Blue samples present larger dispersion.

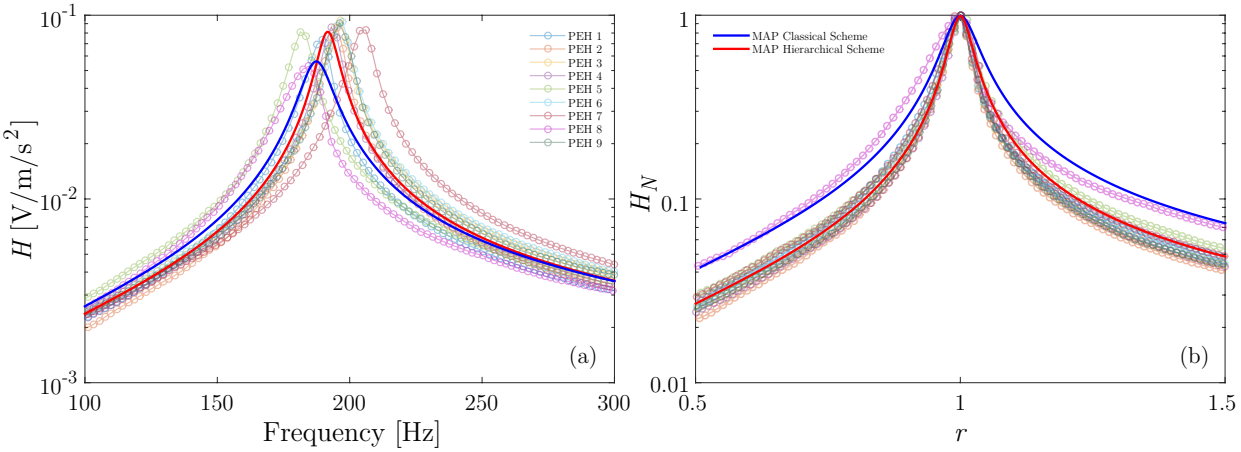

Figure 4.9: Predicted FRF employing MAP values for the posterior distributions of the classical and hierarchical schemes. The FRF is presente in: (a) physical space, and (b) normalized space. Experimental FRFs for the 9 PEHs are presented in circles. MAP prediction of the hierarchical approach fit the experimental observation in both physical and normalized spaces.

4.1.3 Identification of individual PEHs with objective prior

Finally, each device's parameters $\boldsymbol{\theta}_{\mathrm{t}}^{i}$ are updated based on the results of the hierarchical scheme. Now, the posterior distribution for all the data sets $p(\boldsymbol{\theta}_{\mathrm{t}}|\mathbf{D}, M_{hs})$ is taken as an objective prior distribution to update the parameters of each device. Thus, using Eq. (2.18) and the TMCMC method, the posterior distribution for each device $p(\boldsymbol{\theta}_{\mathrm{t}}^{i}|\mathbf{D}^{i}, M_{hs})$ are estimated. The samples obtained for each device, represented with different colors, are shown in Figure 4.10.

As noted, most of the parameters shared similarities across the data sets, except ζ and σ_e for the eighth device. The different behavior of this device explains the gap: it presents a nonlinear behavior (its FRF peak is slightly deviated to the right, please refer to Figure 3.1(a)), inducing the distortion on the named parameters. Even so, the underlying lognormal distribution $p(\boldsymbol{\theta}_{\mathrm{t}}|\mathbf{D}, M_{hs})$ found (Figure 4.6) is able to describe such variations, as it accurately covers the parameter values of the nine devices.

The same comparison between the classical and hierarchical scheme can be made for each device, $p(\boldsymbol{\theta}_{\mathrm{t}}^{i}|\mathbf{D}^{i}, M_{cs})$ and $p(\boldsymbol{\theta}_{\mathrm{t}}^{i}|\mathbf{D}^{i}, M_{hs})$, respectively. For example, in Figure 4.11, the marginalized histograms for the first (i=1) PEH are shown. Again, model parameter dispersions were lower within the hierarchical scheme, which is explained by the different prior distributions employed. Also, note that under both schemes, the prediction error σ_e presented similar distributions, revealing the same data fit for this device. The marginalized histograms of the remaining PEHs are presented in Annex B, since they showed a similar trend.

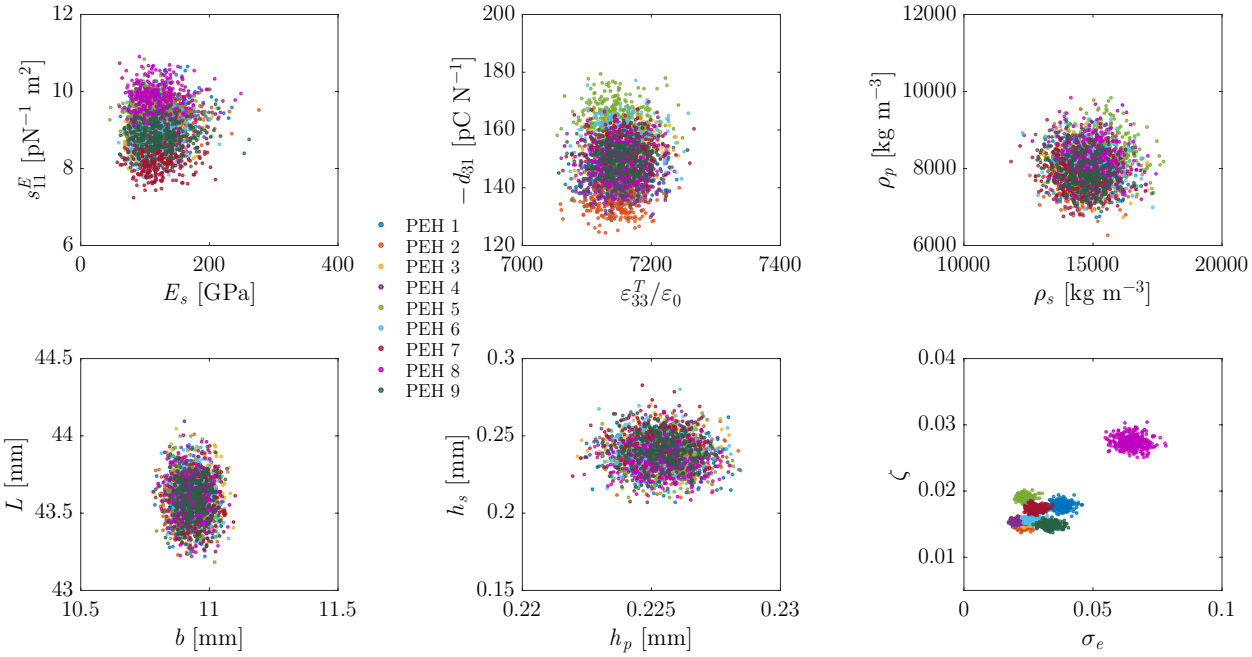

Figure 4.10: Posterior samples for each device under the hierarchical Bayesian scheme.

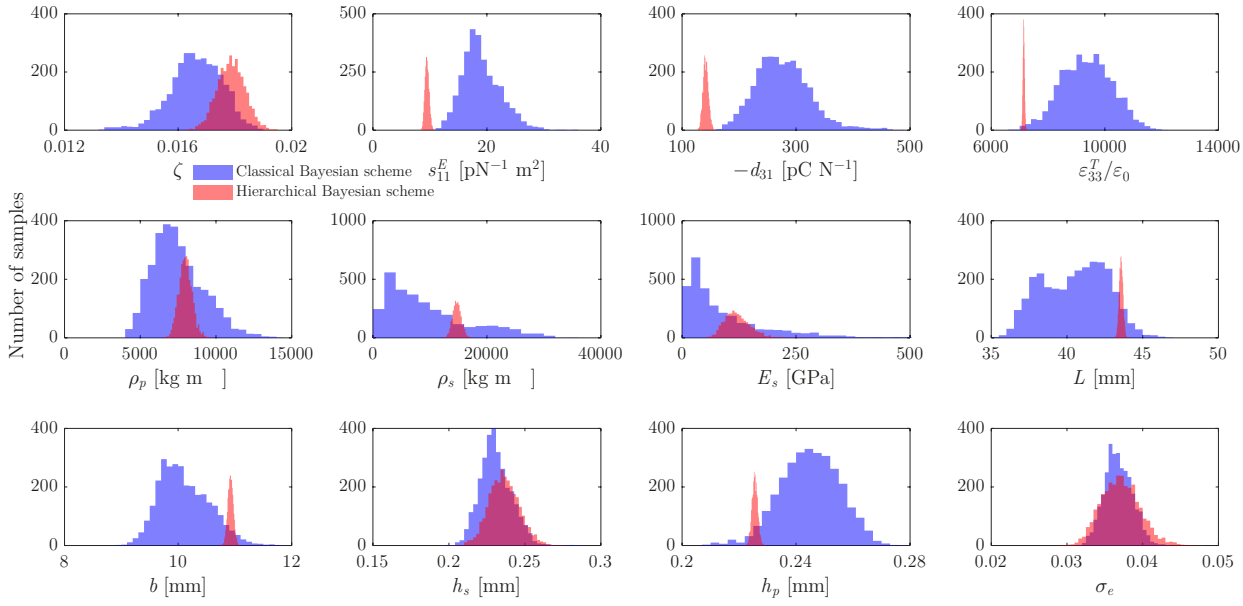

Figure 4.11: Marginalized model parameter histograms of the posterior distribution for the PEH number 1 obtained with the classical (blue) and hierarchical (red) approaches. Blue samples present larger dispersion.

4.2 Model class selection

In order to support the selection of such a classical or hierarchical scheme for PEHs applications, a model class selection procedure is performed following the setting described in Section 2.2.3. Thus, consider the set of models $\{M_j; j = cs, hs\}$ explored in this work and

$P(M_j) = 1/2$. With each model class's evidence, Eq. (2.19) is used to update each model's posterior plausibility. Table 4.4 reports each model's log(evidence) along with its posterior plausibility.

Table 4.4: Model class selection results for the models reviewed.

	M_{cs}	M_{hs}
log(evidence)	-101.04	76.23
$P(M_j\|\mathbf{D})$	0	1

Thus, the model class selection procedure leads to the selection of the hierarchical model. The low value of the evidence in the classical scheme reveals (again) the impact of the prior distribution used $p(\boldsymbol{\theta}_{\mathrm{t}}|M_{cs})$ and the inappropriate formulation of the probabilistic model for multiple PEHs applications.

The same procedure was performed with the individual updating of each data set. Thus, the evidence terms from Eqs. (4.1) and (2.18) were obtained using Eq. (2.27). Table 4.5 shows the results for $\{P(M_j|\mathbf{D}^i); j = cs, hs; i = 1, \ldots, 9\}$, where the hierarchical scheme was preferred in most of the cases. The classical scheme was preferred in the third, sixth, and seventh device, which is explained by the slightly lower value obtained in the prediction error σ_e (please refer to the σ_e histograms of Figures B.2, B.5, and B.6, respectively). The results demonstrate the impact of using an objective prior, such as $p(\boldsymbol{\theta}_{\mathrm{t}}|\mathbf{D}, M_{hs})$.

Table 4.5: Model class selection results for the classical and hierarchical Bayesian schemes when individual data sets are used. The value of $P(M_j|\mathbf{D}^i)$ for each data set is reported together with its respective log-evidence (in parenthesis).

	M_{cs}	M_{hs}
PEH 1	0	1
	(171.444)	(178.483)
PEH 2	0.01	0.99
	(222.704)	(227.289)
PEH 3	0.62	0.38
	(227.073)	(226.371)
PEH 4	0.02	0.98
	(231.965)	(235.630)
PEH 5	0.01	0.99
	(217.992)	(222.990)
PEH 6	0.89	0.11
	(213.148)	(211.084)
PEH 7	1	0
	(219.523)	(206.975)
PEH 8	0.03	0.97
	(114.3641)	(117.852)
PEH 9	0.4	0.6
	(189.253)	(189.673)

Chapter 5

Conclusions

In this work, a hierarchical Bayesian inference framework was proposed, implemented and used to identify electromechanical properties in a group of PEHs based on experimental FRF observations. The framework was illustrated with nine commercial PEHs that share the same nominal properties but present different behaviors due to imperfections in the manufacturing process. The hierarchical framework was compared respect to a classical approach, and the results revealed several important conclusions about the hierarchical Bayesian scheme: (1) it can rigorously account for the uncertainties in model parameters across devices, (2) it can characterize prior distributions to be used in classical Bayesian schemes applied to a single PEH, and (3) it extracts more information about model parameters employing the same observations either at device or group level.

The study started with the implementation of a classical Bayesian scheme to update the model parameters, which required a prior distribution and the formulation of a likelihood function. Here, the prior distribution was selected based on the information given by the manufacturer while the updating was performed adopting TMCMC. Two approaches were explored to characterize the uncertainties in a group of PEHs: (i) updating the model parameters of each device independently and then combining their respective posteriors, and (ii) combining the FRF observations of the PEH group to update the model parameters of a single predictive model. The first approach overestimates the dispersion observed in the experimental FRFs. Additionally, it constitutes a not rigorous procedure, especially in the way in which the posterior distributions of each device are combined. The second approach did not offer a good representation either, as the robust prediction obtained did not capture the variability across the devices. In particular, the FRF dispersion was underestimated.

Given the above, a hierarchical Bayesian scheme for PEHs was proposed by introducing hyperparameters to parameterize the prior distribution. Technical details and estimations that facilitate the implementation of such a hierarchical scheme were presented. The proposed approach leads to a parametric underlying distribution for the model parameters that properly describes the devices' FRF variability observed in experiments. This underlaying distribution was considered to be representative of the electromechanical properties for the group of PEHs studied. A model class selection procedure supported the preference for such a hierarchical scheme (over a classical aproach) for multiple PEHs, which also enabled the

Bayesian identification of individual devices with an objective prior, something unexplored until now. It was proven that under this scheme, a much better account of the model parameter uncertainties was reached, as lower uncertainties were addressed either at device level or group level compared to the classical scheme.

Overall, this study demonstrated the power of the hierarchical Bayesian inference framework proposed for PEHs applications, which was able to identify electromechanical properties of individual and multiple harvesters within a probabilistic approach. Particularly, the proposed hierarchical scheme constitutes a powerful tool to identify electromechanical properties of groups of PEHs, as it enjoys the ability to match the natural frequency, the amplitude at the natural frequency, the FRF shape, and FRF variability observed in experiments.

Bibliography

[1] M. Safaei, H. A. Sodano, and S. R. Anton, "A review of energy harvesting using piezoelectric materials: state-of-the-art a decade later (2008–2018)," *Smart Materials and Structures*, vol. 28, no. 11, p. 113001, 2019.

[2] Z. Zhang, H. Xiang, and Z. Shi, "Modeling on piezoelectric energy harvesting from pavements under traffic loads," *Journal of Intelligent Material Systems and Structures*, vol. 27, no. 4, pp. 567–578, 2016.

[3] Z. Zhang, H. Xiang, Z. Shi, and J. Zhan, "Experimental investigation on piezoelectric energy harvesting from vehicle-bridge coupling vibration," *Energy Conversion and Management*, vol. 163, pp. 169–179, 2018.

[4] A. Erturk and D. J. Inman, *Piezoelectric energy harvesting*. John Wiley & Sons, 2011.

[5] N. E. DuToit and B. L. Wardle, "Experimental verification of models for microfabricated piezoelectric vibration energy harvesters," *AIAA journal*, vol. 45, no. 5, pp. 1126–1137, 2007.

[6] C. D. M. Junior, A. Erturk, and D. J. Inman, "An electromechanical finite element model for piezoelectric energy harvester plates," *Journal of Sound and Vibration*, vol. 327, no. 1-2, pp. 9–25, 2009.

[7] H.-J. Xiang, Z.-W. Zhang, Z.-F. Shi, and H. Li, "Reduced-order modeling of piezoelectric energy harvesters with nonlinear circuits under complex conditions," *Smart Materials and Structures*, vol. 27, no. 4, p. 045004, 2018.

[8] P. Peralta, R. Ruiz, S. Natarajan, and E. Atroshchenko, "Parametric study and shape optimization of piezoelectric energy harvesters by isogeometric analysis and kriging metamodeling," *Journal of Sound and Vibration*, vol. 484, p. 115521, 2020.

[9] A. Erturk and D. J. Inman, "A distributed parameter electromechanical model for cantilevered piezoelectric energy harvesters," *Journal of vibration and acoustics*, vol. 130, no. 4, 2008.

[10] A. Erturk and D. J. Inman, "An experimentally validated bimorph cantilever model for piezoelectric energy harvesting from base excitations," *Smart materials and structures*, vol. 18, no. 2, p. 025009, 2009.

[11] S. C. Stanton, A. Erturk, B. P. Mann, and D. J. Inman, "Nonlinear piezoelectricity in electroelastic energy harvesters: modeling and experimental identification," *Journal of Applied Physics*, vol. 108, no. 7, p. 074903, 2010.

[12] P. Peralta, R. O. Ruiz, and V. Meruane, "Experimental study of the variations in the electromechanical properties of piezoelectric energy harvesters and their impact on the frequency response function," *Mechanical Systems and Signal Processing*, vol. 115, pp. 469–482, 2019.

[13] R. O. Ruiz and V. Meruane, "Uncertainties propagation and global sensitivity analysis of the frequency response function of piezoelectric energy harvesters," *Smart Materials and Structures*, vol. 26, no. 6, p. 065003, 2017.

[14] A. Gelman, J. B. Carlin, H. S. Stern, D. B. Dunson, A. Vehtari, and D. B. Rubin, *Bayesian data analysis*. CRC press, 2013.

[15] C. Papadimitriou, J. L. Beck, and L. S. Katafygiotis, "Asymptotic expansions for reliability and moments of uncertain systems," *Journal of Engineering Mechanics*, vol. 123, no. 12, pp. 1219–1229, 1997.

[16] J. L. Beck and A. Taflanidis, "Prior and posterior robust stochastic predictions for dynamical systems using probability logic," *International Journal for Uncertainty Quantification*, vol. 3, no. 4, 2013.

[17] J. Ching and Y.-C. Chen, "Transitional markov chain monte carlo method for bayesian model updating, model class selection, and model averaging," *Journal of engineering mechanics*, vol. 133, no. 7, pp. 816–832, 2007.

[18] G. Jia, A. A. Taflanidis, and J. L. Beck, "A new adaptive rejection sampling method using kernel density approximations and its application to subset simulation," *ASCE-ASME Journal of Risk and Uncertainty in Engineering Systems, Part A: Civil Engineering*, vol. 3, no. 2, p. D4015001, 2017.

[19] J. L. Beck, "Bayesian system identification based on probability logic," *Structural Control and Health Monitoring*, vol. 17, no. 7, pp. 825–847, 2010.

[20] P. Peralta, R. O. Ruiz, and A. A. Taflanidis, "Bayesian identification of electromechanical properties in piezoelectric energy harvesters," *Mechanical Systems and Signal Processing*, p. 106506, 2020.

[21] A. Poblete, P. Peralta, and R. O. Ruiz, "Tuning nonlinear model parameters in piezoelectric energy harvesters to match experimental data," *ASCE-ASME J Risk and Uncert in Engrg Sys Part B Mech Engrg*, vol. 7, no. 1, 2021.

[22] P. Peralta, R. O. Ruiz, H. Rappel, and S. P. Bordas, "Electromechanical properties identification for groups of piezoelectric energy harvester based on bayesian inference," *Mechanical Systems and Signal Processing*, vol. 162, p. 108034, 2022.

[23] I. Behmanesh, B. Moaveni, G. Lombaert, and C. Papadimitriou, "Hierarchical bayesian

model updating for structural identification," *Mechanical Systems and Signal Processing*, vol. 64, pp. 360–376, 2015.

[24] O. Sedehi, C. Papadimitriou, and L. S. Katafygiotis, "Probabilistic hierarchical bayesian framework for time-domain model updating and robust predictions," *Mechanical Systems and Signal Processing*, vol. 123, pp. 648–673, 2019.

[25] G. C. Ballesteros, P. Angelikopoulos, C. Papadimitriou, and P. Koumoutsakos, "Bayesian hierarchical models for uncertainty quantification in structural dynamics," in *Vulnerability, uncertainty, and risk: quantification, mitigation, and management*, pp. 1615–1624, 2014.

[26] O. Sedehi, C. Papadimitriou, and L. S. Katafygiotis, "Data-driven uncertainty quantification and propagation in structural dynamics through a hierarchical bayesian framework," *Probabilistic Engineering Mechanics*, vol. 60, p. 103047, 2020.

[27] P. D. Congdon, *Bayesian hierarchical models: with applications using R*. CRC Press, 2019.

[28] S. Wu, P. Angelikopoulos, J. L. Beck, and P. Koumoutsakos, "Hierarchical stochastic model in bayesian inference for engineering applications: Theoretical implications and efficient approximation," *ASCE-ASME J Risk and Uncert in Engrg Sys Part B Mech Engrg*, vol. 5, no. 1, 2019.

[29] J. B. Nagel and B. Sudret, "A unified framework for multilevel uncertainty quantification in bayesian inverse problems," *Probabilistic Engineering Mechanics*, vol. 43, pp. 68–84, 2016.

[30] I. Behmanesh and B. Moaveni, "Accounting for environmental variability, modeling errors, and parameter estimation uncertainties in structural identification," *Journal of Sound and Vibration*, vol. 374, pp. 92–110, 2016.

[31] D. Patsialis, A. P. Kyprioti, and A. A. Taflanidis, "Bayesian calibration of hysteretic reduced order structural models for earthquake engineering applications," *Engineering Structures*, vol. 224, p. 111204, 2020.

[32] S. R. Anton and H. A. Sodano, "A review of power harvesting using piezoelectric materials (2003–2006)," *Smart materials and Structures*, vol. 16, no. 3, p. R1, 2007.

[33] K.-V. Yuen, *Bayesian methods for structural dynamics and civil engineering*. John Wiley & Sons, 2010.

[34] W. Betz, I. Papaioannou, and D. Straub, "Transitional markov chain monte carlo: observations and improvements," *Journal of Engineering Mechanics*, vol. 142, no. 5, p. 04016016, 2016.

[35] R. D. Rosenkrantz, *ET Jaynes: Papers on probability, statistics and statistical physics*, vol. 158. Springer Science & Business Media, 2012.

Annexes

Annex A

The expressions for the matrices and vectors are [12]:

$$\mathbf{C}_{eq} = \text{diag}\left[2\zeta_1\omega_1 \;\; 2\zeta_2\omega_2 \;\; \ldots \;\; 2\zeta_{N_o}\omega_{N_o}\right]$$

$$\mathbf{K}_{eq} = \text{diag}\left[\omega_1^2 \;\; \omega_2^2 \;\; \ldots \;\; \omega_{N_o}^2\right]$$

$$\boldsymbol{\chi} = \left[\chi_1 \;\; \chi_2 \;\; \cdots \;\; \chi_{N_o}\right]^{\mathrm{T}}$$

$$\boldsymbol{\varphi} = \left[\varphi_1 \;\; \varphi_2 \;\; \ldots \;\; \varphi_{N_o}\right]^{\mathrm{T}}$$

$$\mathbf{r} = \left[\mathrm{r}_1 \;\; \mathrm{r}_2 \;\; \ldots \;\; \mathrm{r}_{N_o}\right]^{\mathrm{T}}$$

where ζ_n, ω_n, χ_n, φ_n and r_n are the damping ratio, natural frequency, electrical coupling, mechanical coupling, and mechanical forcing terms, respectively, of the $n = \{1, \ldots, N_o\}$ eigenfunction:

$$\phi_n(x) = C_r\left[\cos\left(\frac{\lambda_n}{L}x\right) - \cosh\left(\frac{\lambda_n}{L}x\right) + \sigma_n\left(\sin\left(\frac{\lambda_n}{L}x\right) - \sinh\left(\frac{\lambda_n}{L}x\right)\right)\right]$$

where L is the length of the beam, and σ_n is defined by:

$$\sigma_n = \frac{\sin\lambda_n - \sinh\lambda_n}{\cos\lambda_n + \cosh\lambda_n}$$

$$1 + \cos\lambda_n \cosh\lambda_n = 0$$

while C_r is defined such that the following orthogonality condition is guaranteed:

$$m \int_0^L \phi_n(x)\phi_m(x)dx = \delta_{nm}$$

where $m = b(\rho_s h_s + 2\rho_p h_p)$ is the mass per unit length of the beam and δ_{nm} is the Kronecker delta function, $\delta_{nm} = 1$ if $n = m$ and $\delta_{nm} = 0$ otherwise. With the above, the modal terms can be defined as:

$$\omega_n = \lambda_n^2 \sqrt{\frac{EI}{mL^4}}$$

$$\chi_n = \frac{d_{31}}{s_{11}^E} \frac{b}{h_p} \left(\frac{h_s^2}{4} - \left(h_p + \frac{h_s}{2} \right)^2 \right) \left. \frac{d\phi_n(x)}{dx} \right|_{x=L}$$

$$\varphi_n = \frac{d_{31}}{s_{11}^E} \frac{h_p(h_p + h_s)}{2\varepsilon_{33}^T L} \left. \frac{d\phi_n(x)}{dx} \right|_{x=L}$$

$$\mathrm{r}_n = -m \int_0^L \phi_n(x)dx$$

$$k_{pzt} = \frac{h_p}{2R \left(\varepsilon_{33}^T - \frac{d_{31}^2}{s_{11}^E} \right) bL}$$

where EI is the equivalent bending stiffness of the device:

$$EI = \frac{2b}{3} \left[\frac{E_s h_s^3}{8} + \frac{1}{s_{11}^E} \left(\left(h_p + \frac{h_s}{2} \right)^3 - \frac{h_s^3}{8} \right) \right]$$

Annex B

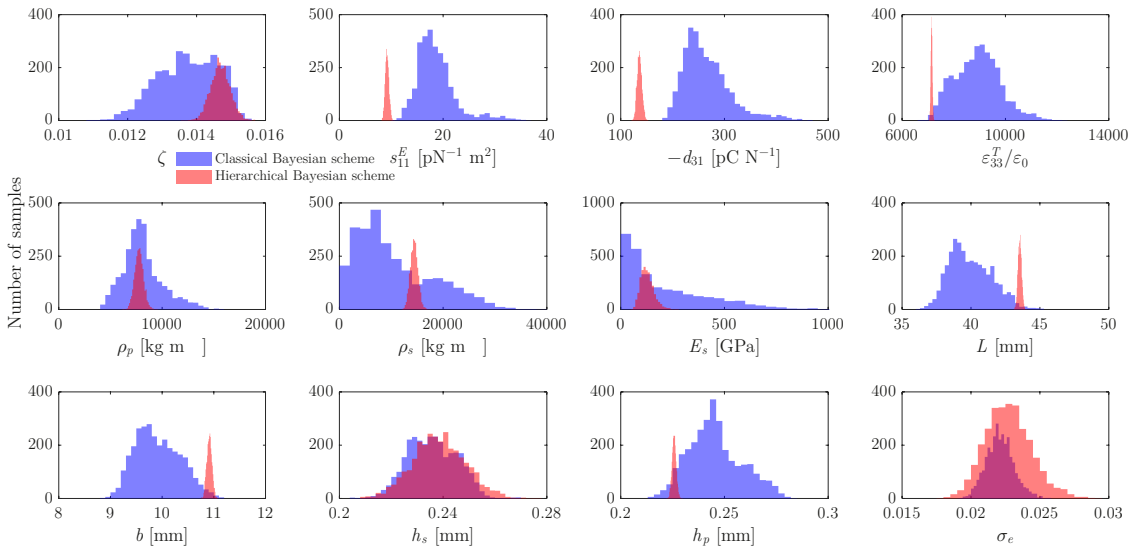

Figure B.1: Marginalized parameter histograms of the posterior distributions obtained with the classical (blue) and hierarchical (red) scheme for the second device.

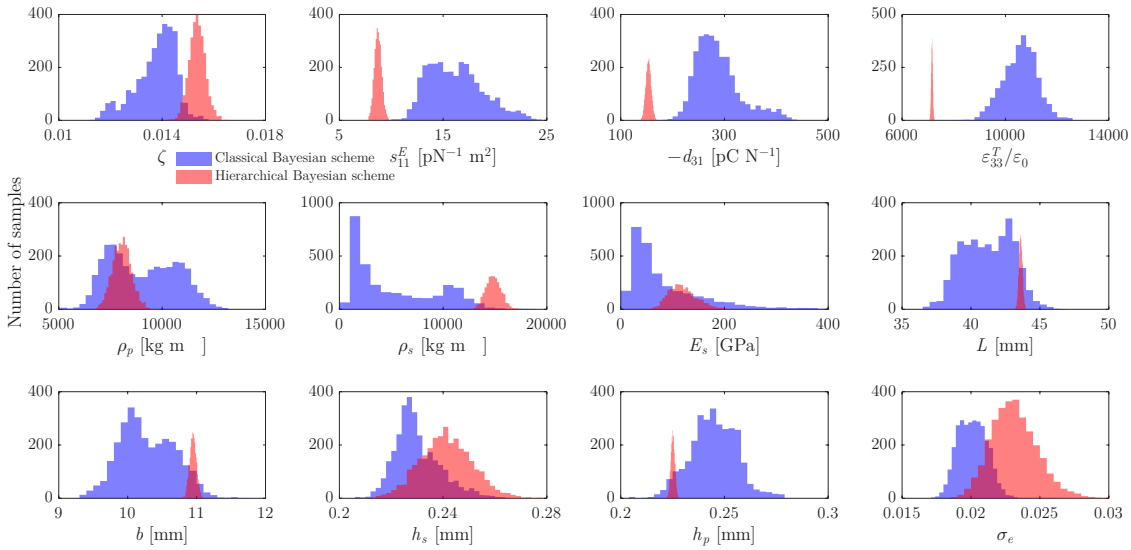

Figure B.2: Marginalized parameter histograms of the posterior distributions obtained with the classical (blue) and hierarchical (red) scheme for the third device.

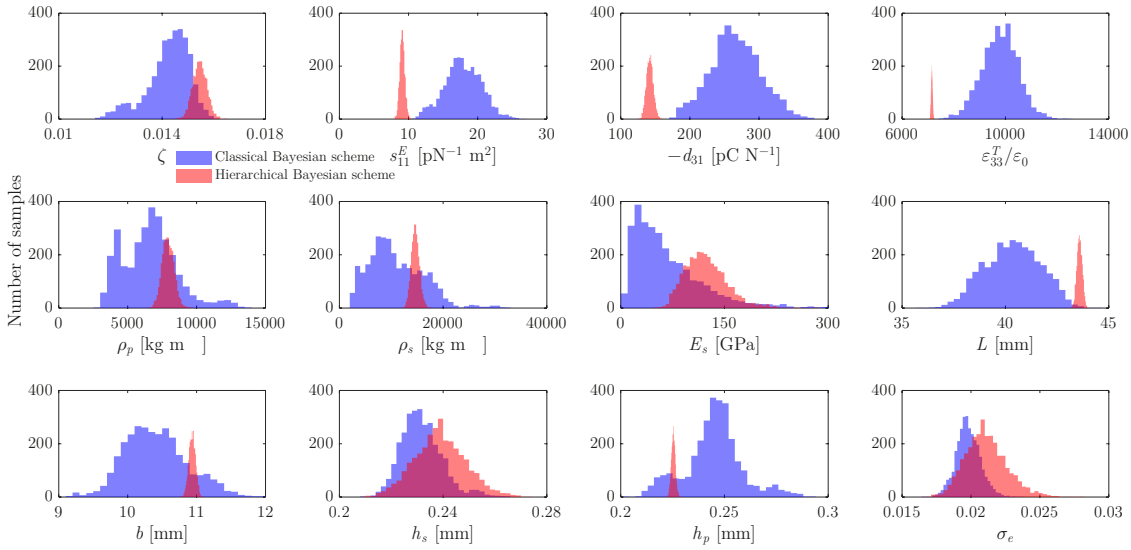

Figure B.3: Marginalized parameter histograms of the posterior distributions obtained with the classical (blue) and hierarchical (red) scheme for the fourth device.

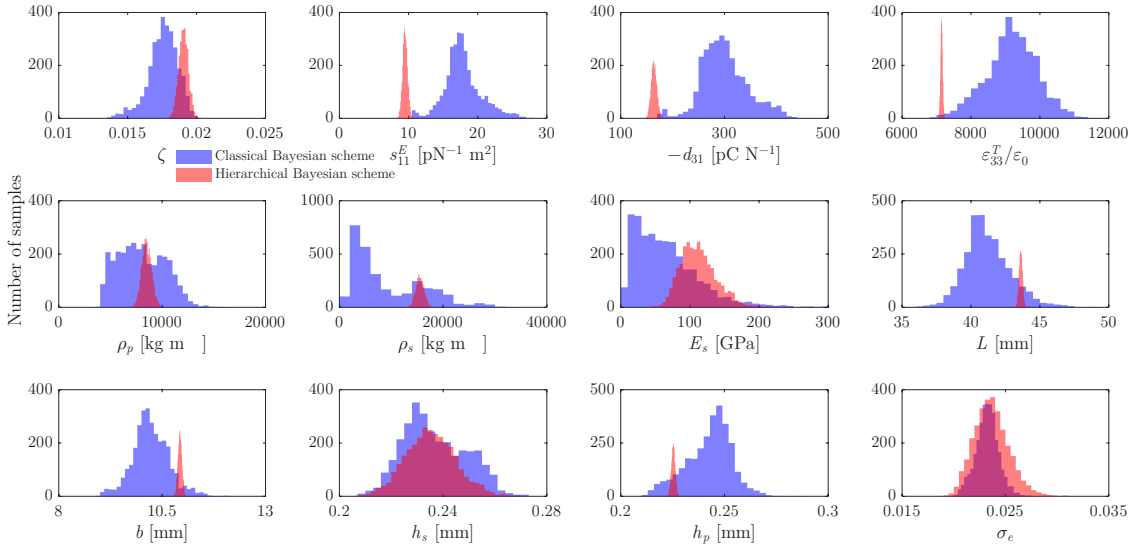

Figure B.4: Marginalized parameter histograms of the posterior distributions obtained with the classical (blue) and hierarchical (red) scheme for the fifth device.

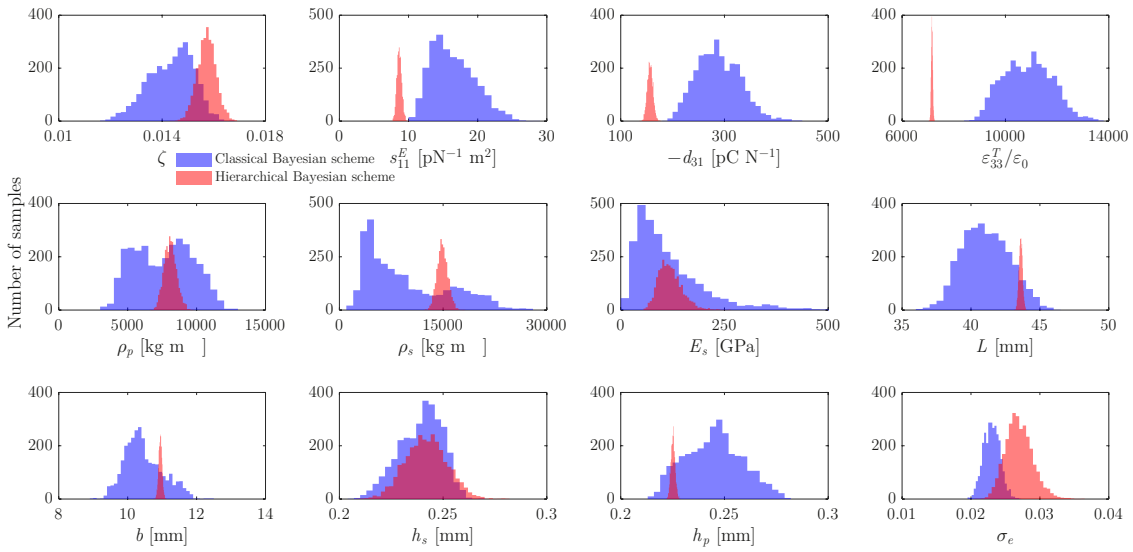

Figure B.5: Marginalized parameter histograms of the posterior distributions obtained with the classical (blue) and hierarchical (red) scheme for the sixth device.

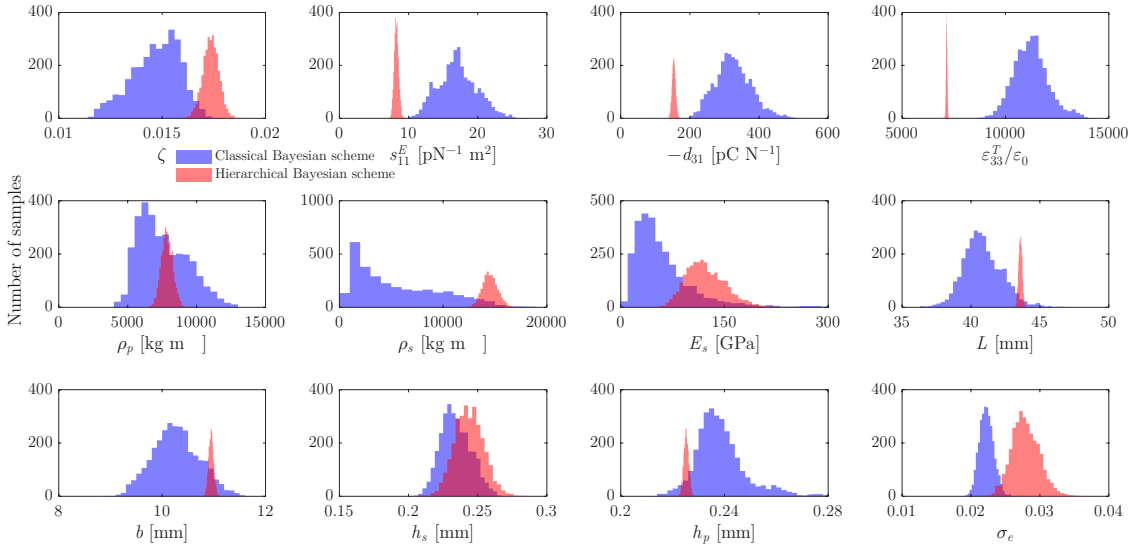

Figure B.6: Marginalized parameter histograms of the posterior distributions obtained with the classical (blue) and hierarchical (red) scheme for the seventh device.

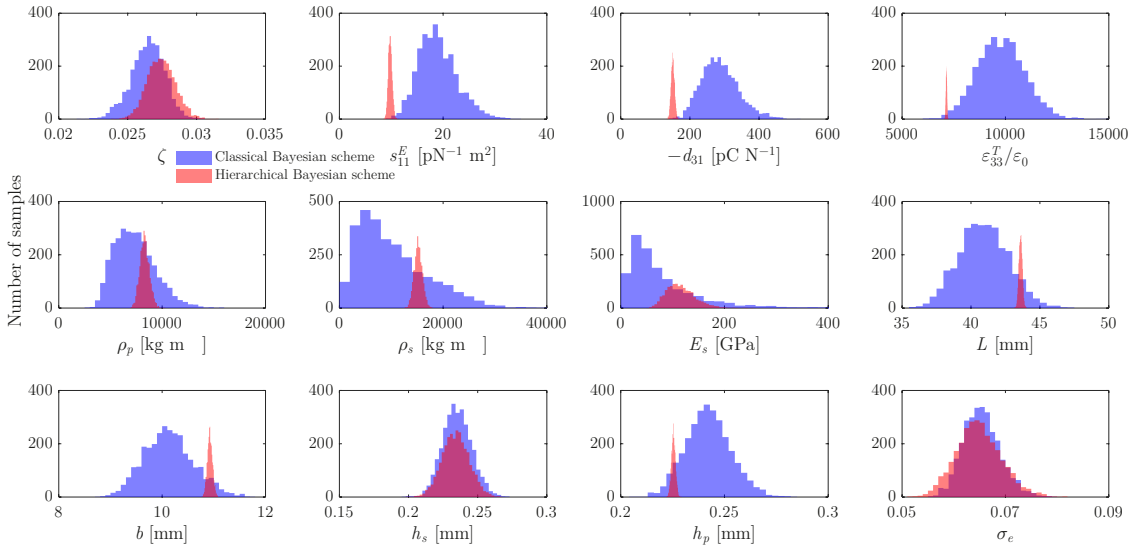

Figure B.7: Marginalized parameter histograms of the posterior distributions obtained with the classical (blue) and hierarchical (red) scheme for the eighth device.

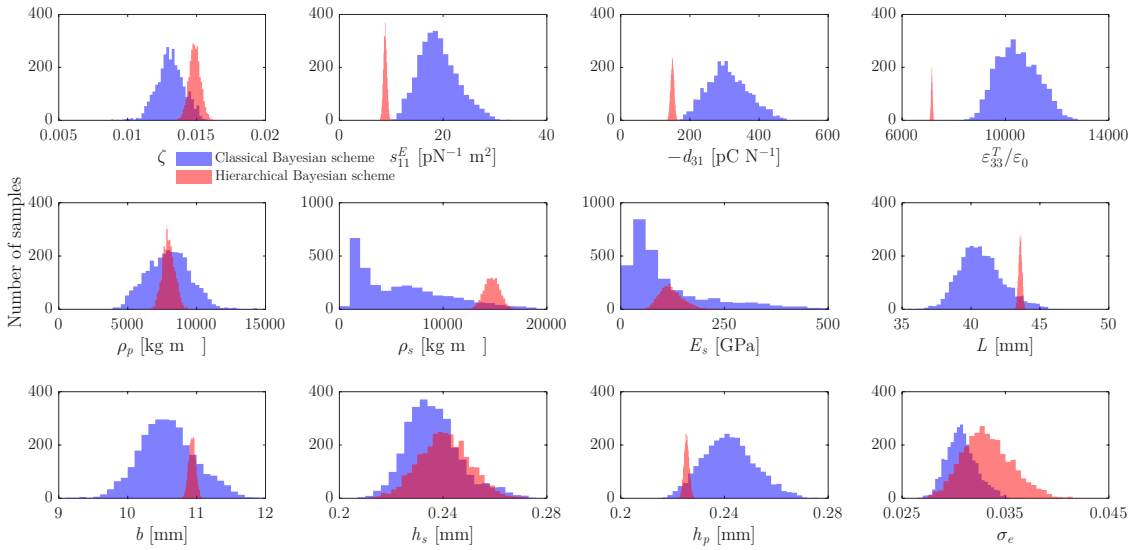

Figure B.8: Marginalized parameter histograms of the posterior distributions obtained with the classical (blue) and hierarchical (red) scheme for the ninth device.